Coherent control of spontaneous emission near a photonic band edge: A qubit for quantum computation

Mesfin Woldeyohannes and Sajeev John
Department of Physics, University of Toronto, 60 St. George Street, Toronto, Ontario, Canada M5S 1A7
(Received 14 May 1999; revised manuscript received 5 August 1999)

We demonstrate the coherent control of spontaneous emission for a three-level atom located within a photonic band-gap structure with one resonant frequency near the edge of the photonic band gap. Spontaneous emission from the three-level atom can be totally suppressed or strongly enhanced depending on the relative phase between the steady-state control laser coupling the two upper levels and the pump laser pulse used to create an excited state of the atom in the form of a coherent superposition of the two upper levels. Unlike the free-space case, the steady-state inversion of the atomic system is strongly dependent on the externally prescribed initial conditions. This nonzero steady-state population is achieved by virtue of the localization of light in the vicinity of the emitting atom. It is robust to decoherence effects provided that the Rabi frequency of the control laser field-atom interaction exceeds the rate of dephasing interactions. As a result, such a system may be relevant for a single-atom, phase-sensitive, optical memory device on the atomic scale. The protected electric dipole within the photonic band gap provides a basis for a qubit to encode information for quantum computations. [S1050-2947(99)08412-7]

PACS number(s): 42.50.Gy, 42.70.Qs

I. INTRODUCTION

Spontaneous emission is a fundamental process resulting from the interaction between radiation and matter. It depends not only on the properties of the excited atomic system but also on the nature of the environment to which that system is optically coupled [1,2]. It is possible to control the rate of spontaneous from an excited atom by altering the density of electromagnetic modes in the neighborhood of the resonant frequency, i.e., by modifying the accessible modes into which the excited atom can radiate. If the modal density in the vicinity of the frequency of interest is less than that of free space, the atomic decay will be retarded, if it is greater it will be accelerated [3].

When the density of electromagnetic modes is a smooth function of frequency over the spectral range of the atomic transition, the rate of spontaneous emission is described by Fermi's golden rule. On the other hand, abrupt changes in the photon density of states (colored vacuum) and photon localization effects [4] may drastically modify the spontaneous emission dynamics. This modification takes the form of long time memory effects and non-Markovian behavior in the atom-reservoir interaction. Strong modification in the local density of electromagnetic modes can be effected by means of photonic crystals. These are dielectric materials in which the refractive index exhibits strong three dimensionally periodic modulation and which in special circumstances may exhibit a photonic band gap (PBG) [5,6]. In carefully engineered semiconductor photonic crystals such as Si, GaP, or Ge, this PBG is centered at roughly twice the index modulation wavelength and extends over a range of frequencies that is approximately 10% of the center frequency of the gap [7]. For the frequency range spanned by a PBG there is no propagating electromagnetic wave in any direction in space. In other words a PBG is a 4π Steradian stop band for some frequency range. Within a PBG the photonic mode density is zero. It has been suggested that this would be accompanied by the inhibition of single-photon spontaneous emission [5], classical light localization [6], a photon-atom bound state [8], fractionalized single-atom inversion, and anomalously large vacuum Rabi splitting [8–10]. In the presence of many atoms, it also leads to anomalously fast collective spontaneous emission rates near the band edge [11] and photon hopping conduction deeper within the gap [12].

The suppression of spontaneous emission combined with the coherent localization of light within a PBG leads to interesting phenomena in quantum optics as well as important technological applications. In the visible and near-infrared wavelength regimes, PBG materials have numerous applications in the telecommunications industry. These applications include the design of zero-threshold, highly efficient microlasers [11], light-emitting diodes that exhibit coherence properties at the single-photon level [13], low-threshold optical switches, and all optical transistors.

The localized mode associated with a defect site in an otherwise perfect photonic crystal, acts as a high-Q microcavity. They are also useful for filters, single-mode masers and lasers. On a more fundamental level, they provide an experimental realization of the Jaynes-Cummings model for cavity quantum electrodynamics (QED) at optical frequencies [14]. Unlike ordinary high-Q microcavity resonators, localized states in a PBG may extend over many optical wavelengths. These localized states facilitate coherent energy transport and cooperative effects on a scale much larger than the optical wavelength. This leads to a host of fundamentally new effects in quantum optics. The ability to selectively control spontaneous emission, while at the same time preserving propagative effects over many wavelengths, is a unique feature of PBG systems.

Just as point defects in a photonic crystal are used to trap light, extended defects can be used to guide light from one location to another. Extended defects (such as a line of point defects) can be engineered for the purpose of wave guiding through the otherwise impenetrable PBG [15,16]. In large-scale PBG materials made from self-assembly methods, re-

 ©1999 The American Physical Society

gions of crystalline order are separated by grain boundaries. These planar defects may likewise act as waveguiding paths within the PBG. Engineered line defects and planar defects can be used to guide light between individual microcavity devices, thereby allowing the PBG material to act as a host for integrated optical circuits.

Small-scale photonic crystals with complete three-dimensional (3D) gaps at microwave frequencies have already been realized [17] by direct drilling methods, and large-scale two-dimensional PBG systems have been produced in the near infrared [18] using electrochemical etching methods. The outstanding problem in the field is the microfabrication of large-scale photonic crystals with full three-dimensional band gaps at infrared and optical frequencies. To achieve band gaps for the infrared and visible spectra several challenges exist. The periodicity of the crystal should be on the scale of the wavelength of light (about 500 nm), both constituent materials of the crystal should be topologically interconnected [19], and the ratio of their refractive indices n should be close to 3.0 [7]. Two approaches are currently being employed to create photonic crystals. The first one is engineering by microlithography [20,21]. However, it is very cumbersome and expensive to extend this microengineering method to produce large-scale 3D structures with periodicity on the scale of the wavelength of visible light [22]. The second approach involves self-organizing systems such as colloidal crystals [23–25] and artificial opals [26–28] as templates for PBG microfabrication. Monodisperse colloidal suspensions of latex microspheres and SiO_2 spheres (opals) can sediment into crystalline structures with excellent long-range periodicity at optical length scales [25]. Colloidal crystal growth produces inherently three-dimensional structures, a significant advantage over lithographic techniques which primarily produce two-dimensional patterns. However, neither colloids nor opals (close-packed fcc lattice of SiO_2 spheres) achieve the high refractive index ratios and interconnectedness necessary for photonic band-gap formation. Therefore, it is necessary to invert the structure by infiltrating the template with a high refractive index semiconductor such as GaP, Si, or Ge. The original template may be finally removed by chemical or heat treatment. It has been demonstrated theoretically [7] that such structures exhibit near-visible photonic band gaps on the scale of 10% of of the gap frequency. This type of ''inverted'' opal structure was experimentally realized in Ref. [29], where a closed-packed fcc lattice of air spheres in TiO_2 (refractive index $n=2.8$) is reported. A similar structure made of carbon was reported [30] using an artificial opal template. Most recently, an inverse opal consisting of CdSe was realized [31]. Such macroporous crystals suggest the feasibility of producing a new class of 3D photonic crystals for the optical spectrum. Structures of this type made out of GaP or Si would be relevant to quantum optical experiments in which atoms, dye molecules, or other active materials are inserted into specific locations within the photonic crystal.

The absence of single-photon spontaneous emission for an isolated atom in a PBG guarantees that the emitted photon remains partially localized in the vicinity of the emitting atom leading to the formation of a photon-atom bound state [8]. On the other hand, driving an atom with a sufficiently strong resonant field alters the radiative dynamics in a fundamental way [32,33], even in ordinary vacuum [34–36]. It leads to such interesting effects as the enhancement of the index of refraction with greatly reduced absorption [37], electromagnetically induced transparency [38] and optical amplification without population inversion [39]. The coherent control of molecular chemical reactions [40] is an emerging frontier in chemical physics [41]. Using the coherence properties of an external laser-field-driven interaction, radiatively controlled chemical pathways can be enhanced or retarded by quantum-mechanical interference effects. Selective photodissociation of molecules mediated by the interference between two two-photon excitation processes has been reported [42]. Coherent control of current in a semiconductor has also been demonstrated [43]. Here the direction of the electrical current, formed by interband transitions in a bulk semiconductor via coherent one- and two-photon absorption, is controlled by simply adjusting the relative phase of the two beams that are optically generating carriers across the gap. In view of these achievements, it is of great interest to consider the combined effects of coherent control by means of external laser fields and the coherent localization effects facilitated by a photonic band gap.

In this paper we study the combined effects of coherent control and photon localization on spontaneous emission from a three-level atom with one resonant frequency at or near the edge of a PBG. We demonstrate that storage of quantum information in a single atom is facilitated by the localization of light in the vicinity of the atom when one of the atomic transitions lies within a photonic band gap. The nature of this information is controlled by the combination of quantum interference between different radiative pathways within the atom mediated by the external laser field and photon localization effects mediated by the PBG. In our model system, a pump laser pulse is used to create an excited state of the atom as a coherent superposition of the two upper levels. A control, cw, laser field with a specific phase relation to the pump laser pulse stimulates radiative transitions between the upper two excited states. It is shown that spontaneous emission can be totally suppressed or strongly enhanced by changing the relative phase between the control laser field and the initial atomic Bloch vector determined by the pump laser pulse. Unlike the free-space case, the steady-state inversion of the atomic system is strongly dependent on the externally prescribed initial conditions. As a result, such a system may be relevant for a single-atom, phase-sensitive, optical memory device on the atomic scale.

Provided that coherence can be maintained between the atomic levels $|2\rangle$ and $|3\rangle$, our model system can also act as a qubit (two-state system) to encode information for quantum computation. In our scheme, coherence is forced on the atomic system by means of the control laser field. Two or more such systems can be used to construct quantum logic gates [44]. At the heart of quantum computation is the entanglement of many qubits which form the register of the quantum computer. To create and maintain such a highly entangled state, the qubits must be strongly coupled to one another and to an external field. Yet coupling to other external influences must be minimized since it leads to decoherence. Random perturbations from the environment cause a pure quantum state to evolve to a mixture of states and thereby lose its key properties of interference and entanglement. The PBG material provides an ideal environment to

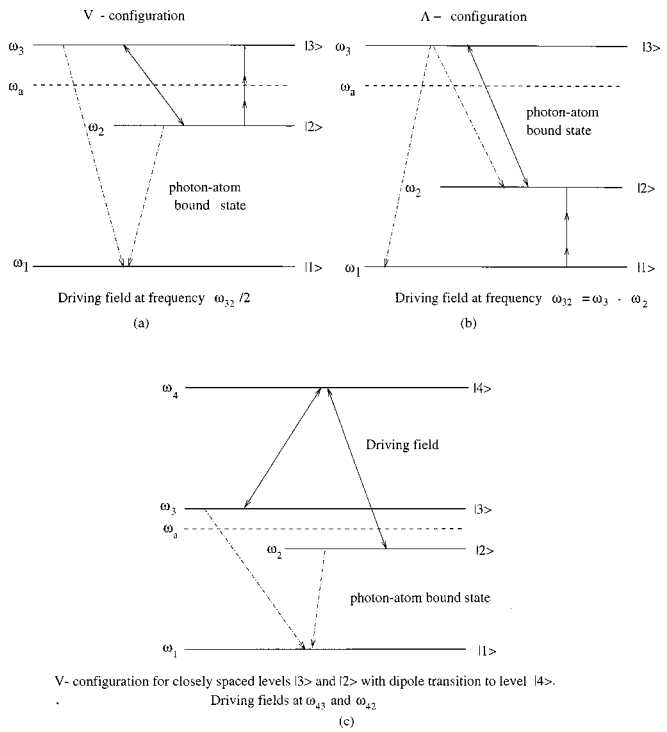

FIG. 1. Schematic representations of a driven three-level system (a) in the V configuration and (b) in the Λ configuration. The transition frequency ω_{31} is near the band-edge frequency ω_a of a PBG. Lines with arrows at both ends denote the control laser field of Rabi frequency Ω driving the transition $|3\rangle \leftrightarrow |2\rangle$. Double-arrowed lines denote two-photon transitions. Dot-dashed lines denote dipole allowed transitions. In the V configuration levels $|3\rangle$ and $|2\rangle$ are of the same symmetry, and ω_{21} is deep inside the PBG so that there are no single-photon spontaneous emissions on the transitions $|3\rangle \rightarrow |2\rangle$ and $|2\rangle \rightarrow |1\rangle$. Similarly in the Λ configuration levels $|2\rangle$ and $|1\rangle$ are of the same symmetry, and ω_{32} is deep inside the PBG so that there are no single-photon spontaneous emissions on the transitions $|3\rangle \rightarrow |2\rangle$ and $|2\rangle \rightarrow |1\rangle$. The control laser field drives a two-photon transition ($2\omega_L = \omega_{32}$) in the V configuration and a single-single photon transition ($\omega_L = \omega_{32}$) in the Λ configuration. (c) shows indirect coupling of levels $|2\rangle$ and $|3\rangle$ in a V system via another level $|4\rangle$. Such a scheme will allow as to strongly couple levels $|2\rangle$ and $|3\rangle$ even when the transition ω_{32} lies in the infrared or far infrared.

satisfy these seemingly contradictory requirements by preserving the resonance dipole-dipole interaction between neighboring qubits [12,8] while at the same time shielding them from the external environment (radiation reservoir).

II. MODEL

A. Description of the model

The physical system we consider consists of a single three-level atom placed inside a photonic crystal which is then driven by a laser field, see Fig. 1. We let $|1\rangle$ denote the ground level of the atom, and $|2\rangle$ and $|3\rangle$ the two excited levels with orthonormality conditions $\langle i|j\rangle = \delta_{ij}$, where δ_{ij} is the Krönecker delta function. We designate the energy of level $|i\rangle$ by $\hbar\omega_i$ and the frequency separation between level $|i\rangle$ and $|j\rangle$ by $\omega_{ij} = \omega_i - \omega_j$. The transition between levels can be described using the atomic operators $\sigma_{ij} = |i\rangle\langle j|$. Using the property $\sigma_{ij}|k\rangle = \delta_{jk}|i\rangle$, it follows that

$$[\sigma_{ij}, \sigma_{lk}] = \delta_{jl}\sigma_{ik} - \delta_{ik}\sigma_{lj}. \tag{1}$$

We choose to work in Schrödinger picture of quantum mechanics, where operators are treated as time independent. The upper atomic level $|3\rangle$ is dipole coupled to the ground level $|1\rangle$ by radiation modes (photon reservoir) in a three-dimensional periodic dielectric structure. The transition frequency ω_{31} is assumed to be near the edge of the gap in the density of the reservoir photon modes. Each mode of the photon reservoir is characterized by a wave vector $\mathbf{k}$ and a polarization index $\lambda (= 1,2)$, and can be treated as a quantum oscillator with frequency ω_k. Transitions between photon occupation number states $|n_{\mathbf{k}\lambda}\rangle$ are described by the radiation field annihilation ($a_{\mathbf{k}\lambda}$) and creation ($a^{\dagger}_{\mathbf{k}\lambda}$) operators satisfying the standard Bose algebra $[a_{\mathbf{k}\lambda}, a^{\dagger}_{\mathbf{k}'\lambda'}] = \delta_{\mathbf{k}\mathbf{k}'}\delta_{\lambda\lambda'}$. All atomic operators σ_{ij} commute with all operators ($a_{\mathbf{k}\lambda}$ and $a^{\dagger}_{\mathbf{k}\lambda}$) for the quantized electromagnetic oscillator.

In our model system we assume that the transition $|3\rangle \rightarrow |2\rangle$ between the two upper levels is driven by a resonant control laser field of angular frequency ω_L, Rabi frequency Ω, and phase ϕ_L. The Rabi frequency Ω characterizes the strength of the driving field, and is given by the product of the transition dipole moment and the driving field amplitude (i.e., the square root of the field intensity). We also assume that spontaneous emission on the transitions $|3\rangle \rightarrow |2\rangle$ and $|2\rangle \rightarrow |1\rangle$ is inhibited either by symmetry considerations or by the presence of the photonic band gap.

If the three level atom is in the so-called V configuration [Fig. 1(a)], the upper levels $|3\rangle$ and $|2\rangle$ are of the same symmetry, and single-photon spontaneous emission $|3\rangle \rightarrow |2\rangle$ is not dipole allowed. If we further assume that transition frequency ω_{21} is deep inside the gap, then single-photon spontaneous emission for the transition $|2\rangle \rightarrow |1\rangle$ will lead to a photon-atom bound state [10,45]. In such a V system, the external control laser field of frequency ω_L which couples levels $|3\rangle$ and $|2\rangle$ drives a two-photon transition ($2\omega_L = \omega_{32}$), since the levels are of the same symmetry. From a practical point of view, we want the transition frequency ω_{32} to be as large as possible, as it may be difficult to generate microwave fields of sufficient amplitude to drive the required two-photon transition. However, the magnitude of ω_{32} is restricted by the width of the photonic band gap. For a gap centered at frequency ω_o and with a gap-to-midgap ratio of $r \equiv \Delta\omega/\omega_o$, conditions that ω_{31} be near the edge of the gap and that ω_{21} be deep inside the gap require that $\omega_{32} = \omega_{31} - \omega_{21} < r\omega_o$. Thus to make ω_{32} large we need a gap with as high a central frequency as possible and as large a width as possible. For a gap centered at an optical frequency $\omega_o \sim 10^{15}$ Hz and with a gap-to-midgap ratio of 10%, the frequency separation ω_{32} between levels $|3\rangle$ and $|2\rangle$ must be approximately 5×10^{13} Hz.

Another means of overcoming the above practical limitation associated with the V system is to couple levels $|2\rangle$ and $|3\rangle$ indirectly by way of a transition to a higher level $|4\rangle$ which lies far above level $|3\rangle$. This will allow us to both strongly couple levels $|2\rangle$ and $|3\rangle$ and use a narrow-band gap, even when the transition frequency ω_{32} lies in the near

or far infrared. Level $|4\rangle$ is dipole coupled to level $|2\rangle$ (and hence to level $|3\rangle$, since they are of the same symmetry) and the transitions ω_{42} and ω_{43} are both in the visible and both lie outside the gap, as shown in Fig. 1(c). The transition ω_{42} is then pumped by a resonant laser $\omega_p=\omega_{42}$ followed by a stimulated emission into level $|3\rangle$ using a laser which couples levels $|4\rangle$ and $|3\rangle$ [46].

On the other hand, for a three level system in the Λ configuration [Fig. 1(b)], levels $|2\rangle$ and $|1\rangle$ have the same symmetry and there is no dipole-allowed single-photon spontaneous emission between these levels. If we further assume that the transition frequency ω_{32} is far inside the gap, the dipole-allowed transition $|3\rangle\rightarrow|2\rangle$ will create a photon-atom bound state whose radiative lifetime is given by the two-photon spontaneous emission time for the $|2\rangle\rightarrow|1\rangle$ transition. To reconcile the conditions that ω_{31} is near the band edge and that ω_{32} is deep in the gap, we require that $\omega_{21}=\omega_{31}-\omega_{32}\leqslant r\omega_o$. Given the practical fact that $r\leqslant 0.1$, it follows that levels $|2\rangle$ and $|1\rangle$ should be close to each other but both far from level $|3\rangle$, as shown in Fig. 1(b). This, in turn, will reduce the decay rate of the photon-atom bound state due to two-photon spontaneous emission from $|2\rangle\rightarrow|1\rangle$. However, since ω_{32} is within the gap, the control laser driving the single-photon transition $|3\rangle\rightarrow|2\rangle$ must be injected by means of engineered or naturally occurring defect or waveguide modes within the band-gap material.

Our model system may be realized by trapping cold atoms in the void regions of a photonic crystal, using the properties of the electromagnetic eigenmodes of a 3-d PBG material. If the PBG material is illuminated by an intense laser field with frequency near the bottom of the ''air'' band, a nearly standing-wave electromagnetic field will arise with strong electric-field gradients and peak intensities that lie in the void fraction of the material. This field distribution will act as an optical trapping potential for a cold atom vapor [47]. This will trap atoms in the void regions of the photonic crystal where the field is most intense, and prevent the atoms from colliding with the dielectric backbone of the PBG material. In a typical 3-d PBG material, the void fraction forms a connected network that accounts for nearly 75% of the volume of the material. Atoms which are optically trapped in this extensive void network will be immune to collisional dephasing and decoherence phenomena arising form direct interaction with atoms in the solid dielectric backbone. Another way of realizing our model system is by doping the solid fraction of the PBG material with an impurity three-level atom such as a rare-earth atom or by means of a quantum dot (artificial atom) incorporated inside the semiconducting backbone of the photonic crystal with the required electronic transitions near the photonic band edge. However, in either of these latter cases, decoherence effects arising from the interaction of the three-level system with phonons in the dielectric fraction of the PBG material need to be carefully considered.

B. Model Hamiltonian

The total Hamiltonian H of our model system can be written as the sum of the atomic Hamiltonian

$$H_A=\sum_{i=1}^{3}\hbar\omega_i\sigma_{ii} \tag{2}$$

of the field Hamiltonian (neglecting the zero-point energy)

$$H_F=\sum_{\lambda=1}^{2}\sum_{\mathbf{k}}\hbar\omega_k a_{\mathbf{k}\lambda}^{\dagger}a_{\mathbf{k}\lambda}, \tag{3}$$

the total interaction Hamiltonian between the atom and the photon reservoir (which is responsible for spontaneous as well as stimulated emission),

$$H_{AF}=i\hbar\sum_{\lambda=1}^{2}\sum_{\mathbf{k}}g_{\mathbf{k}\lambda}(a_{\mathbf{k}\lambda}^{\dagger}\sigma_{13}-\sigma_{31}a_{\mathbf{k}\lambda}), \tag{4}$$

and the interaction Hamiltonian between the atom and the coherent monochromatic laser field (treated as a classical field):

$$H_{AL}=i\hbar\Omega[e^{i(\omega_L t+\phi_c)}\sigma_{23}-e^{-i(\omega_L t+\phi_c)}\sigma_{32}]. \tag{5}$$

Here $g_{\mathbf{k}\lambda}$ is the frequency-dependent coupling constant (assumed to be real) between the atomic transition $|3\rangle\rightarrow|1\rangle$ and the mode $\{\mathbf{k}\lambda\}$ of the radiation field:

$$g_{\mathbf{k}\lambda}=\frac{\omega_{31}d_{31}}{\hbar}\left(\frac{\hbar}{2\epsilon_o\omega_{\mathbf{k}}V}\right)^{1/2}\hat{\mathbf{e}}_{\mathbf{k}\lambda}\cdot\hat{\mathbf{d}}_{31}. \tag{6}$$

Also, d_{31} and $\hat{\mathbf{d}}_{31}$ are the magnitude and unit vector of the atomic dipole moment $\mathbf{d}_{31}$ for the transition $|3\rangle\rightarrow|1\rangle$, V is the sample volume, $\hat{\mathbf{e}}_{\mathbf{k}\lambda}$ are the two transverse (polarization) unit vectors, and ϵ_o is the Coulomb constant. The coupling constant $g_{\mathbf{k}\lambda}$ fully characterizes the density of modes in the photon reservoir. In the framework of perturbation theory, which is usually employed in quantum electrodynamics, the sum $H_0=H_A+H_F$ is regarded as the Hamiltonian of the unperturbed system whereas the sum $H_I=H_{AF}+H_{AL}$ describes the perturbation. The total Hamiltonian of the system is then

$$H=H_0+H_I. \tag{7}$$

The interaction Hamiltonians H_{AF} and H_{AL} are written in electric dipole approximation. H_{AF} and H_{AL} are also written in the rotating-wave approximation, which neglects virtual processes of excitation (de-excitation) of the atom with simultaneous creation (annihilation) of a photon.

We refer to the model Hamiltonian (7) as describing the ''leading approximation'' to our physical model system. In this leading approximation a number of spontaneous emission effects and nonradiative interactions are neglected. In particular, the spontaneous emission channels $|3\rangle\rightarrow|2\rangle$ and $|2\rangle\rightarrow|1\rangle$ are absent in Eq. (7). We demonstrate in what follows that for coherent control in a PBG material, this leading approximation describes the essential physics. In Sec. V and VI we consider the corrections to this leading approximation.

We assume that the radiation-field reservoir is initially in the vacuum state. At $t=0$, an ultrashort pumping laser pulse is used to prepare the atom in a coherent superposition of its two upper levels $|2\rangle$ and $|3\rangle$ in the form

$$|\Psi(0)\rangle=\cos\theta|3,\{0\}\rangle+e^{i\phi_p}\sin\theta|2,\{0\}\rangle. \tag{8}$$

Here the state vector $|j,\{0\}\rangle \equiv |j\rangle|\{0\}\rangle$ represents the atom in the upper states $|j\rangle$ and the vacuum electromagnetic field (that is no photons present). The state $|j,\{0\}\rangle$ is a direct product of the atomic state $|j\rangle$ and the radiation state $|\{0\}\rangle$, since the atomic operators are assumed to commute with the radiation field operators.

With the above initial condition, the system evolution may be described using the basis states of the unperturbed Hamiltonian H_0, listed below together with their corresponding eigenvalues:

$$|3,\{0\}\rangle, \quad \hbar\omega_3, \tag{9a}$$

$$|2,\{0\}\rangle, \quad \hbar\omega_2, \tag{9b}$$

$$|1,\{1_{\mathbf{k}\lambda}\}\rangle, \quad \hbar(\omega_1+\omega_k). \tag{9c}$$

Here the state vector $|1,\{1_{\mathbf{k}\lambda}\}\rangle$ represents the atom in the ground state $|1\rangle$ and a single photon in a mode $\{\mathbf{k}\lambda\}$. The vectors $|2,\{1_{\mathbf{k}\lambda}\}\rangle$ are assumed to be inaccessible in the V system, since there is no single-photon spontaneous emission on the transition $|3\rangle \rightarrow |2\rangle$. Two-photon spontaneous emission is considered to be negligible compared to the two-photon stimulated emission from $|3\rangle$ to $|2\rangle$, induced by the classical control laser field. This latter effect is described by the classical Rabi field (two-photon transition) amplitude $\hbar\Omega e^{i(\omega_L t+\phi_L)}$. Similarly, in the Λ system, single-photon spontaneous emission from $|3\rangle$ to $|2\rangle$, although allowed, is assumed to be negligible compared to stimulated emission driven by the control laser field. For the Λ system, the effects of stimulated emission are described by the classical Rabi field (one-photon transition) amplitude $\hbar\Omega e^{i(\omega_L t+\phi_L)}$. It follows that the excitation number

$$N=|3,\{0\}\rangle\langle 3,\{0\}|+|2,\{0\}\rangle\langle 2,\{0\}|+\sum_{\lambda=1}^{2}\sum_{\mathbf{k}} a^{\dagger}_{\mathbf{k}\lambda}a_{\mathbf{k}\lambda} \tag{10}$$

is a constant of the motion of the total Hamiltonian H.

In the course of time, the initial state vector $|\Psi(0)\rangle$ develops according to the Schrödinger equation into some linear combination of the states $|j,\{0\}\rangle$ with the accompanying spontaneous emission of a photon into the state $|1,\{\mathbf{k}\lambda\}\rangle$. Accordingly, the state vector will be written as

$$|\Psi(t)\rangle = b_3(t)e^{-i\omega_3 t}|3,\{0\}\rangle + b_2(t)e^{-i\omega_2 t}|2,\{0\}\rangle + \sum_{\mathbf{k}\lambda} b_{1\mathbf{k}\lambda}(t)e^{-i(\omega_{\mathbf{k}}+\omega_1)t}|1,\{\mathbf{k}\lambda\}\rangle, \tag{11}$$

with the amplitudes $b_{2,3}(t)$ and $b_{1\mathbf{k}\lambda}(t)$ determined by the Schrödinger equation. In writing the general state vector (11), the time dependences of the amplitudes due to the unperturbed Hamiltonian H_0 are explicitly factored out in the form of exponentials. Comparing Eqs. (11) and (8), we obtain

$$b_3(0)=\cos\theta, \tag{12a}$$

$$b_2(0)=e^{i\phi_p}\sin\theta, \tag{12b}$$

$$b_{1\mathbf{k}\lambda}(0)=0 \tag{12c}$$

as the initial values for the amplitudes $b_{2,3}(t)$ and $b_{1\mathbf{k}\lambda}(t)$ corresponding to the initial state (8). Conservation of probability requires that

$$\langle\Psi(t)|\Psi(t)\rangle = |b_3(t)|^2+|b_2(t)|^2+\sum_{\mathbf{k}\lambda}|b_{1\mathbf{k}\lambda}(t)|^2=1. \tag{13}$$

C. Equations of motion

Using Eqs. (7) and (11) in the Schrödinger equation $i\hbar(d/dt)|\Psi(t)\rangle = H|\Psi(t)\rangle$, and projecting the result onto $|1,\{\mathbf{k}\lambda\}\rangle$, $|2,\{0\}\rangle$, and $|3,\{0\}\rangle$, respectively, we obtain the following (infinite) set of coupled equations for the amplitudes $b_{2,3}(t)$ and $b_{\mathbf{k}\lambda}(t)$:

$$\dot{b}_{1\mathbf{k}\lambda}(t)=g_{\mathbf{k}\lambda}b_3(t)e^{i\mu_{\mathbf{k}}}, \tag{14a}$$

$$\dot{b}_2(t)=\Omega e^{i\phi_c}b_3(t), \tag{14b}$$

$$\dot{b}_3(t)=-\Omega e^{-i\phi_c}b_2(t)-\sum_{\mathbf{k}\lambda} g_{\mathbf{k}\lambda}b_{1\mathbf{k}\lambda}(t)e^{-i\mu_{\mathbf{k}}t}, \tag{14c}$$

where the dot over an amplitude signifies the time derivative, and

$$\mu_{\mathbf{k}}=\omega_{\mathbf{k}}-\omega_{31} \tag{15}$$

is the detuning of the radiation mode frequency $\omega_{\mathbf{k}}$ from the atomic transition frequency ω_{31}. Equation (14a) can be integrated (in time), using the initial condition $b_{1\mathbf{k}\lambda}(0)=0$, to give

$$b_{1\mathbf{k}\lambda}(t)=g_{\mathbf{k}\lambda}\int_0^t b_3(t')e^{i\mu_{\mathbf{k}}t'}dt'. \tag{16}$$

Substituting this expression for $b_{1\mathbf{k}\lambda}(t)$ in Eqs. (14b) and (14c) then yields the following two coupled integrodifferential equations:

$$\dot{b}_2(t)=\Omega e^{i\phi_c}b_3(t), \tag{17a}$$

$$\dot{b}_3(t)=-\Omega e^{-i\phi_c}b_2(t)-\int_0^t G(t-t')b_3(t')dt', \tag{17b}$$

where

$$G(t-t')=\sum_{\mathbf{k}\lambda} g^2_{\mathbf{k}\lambda}e^{-i\mu_{\mathbf{k}\lambda}(t-t')} \tag{18}$$

is the delay Green's function of the problem. In writing down Eqs. (17a) and (17b), we have exchanged the order of summation over $\mathbf{k}\lambda$ and integration over time. The resulting Green's function depends very strongly on the photon density of states of the reservoir. In essence, $G(t-t')$ is a measure of the photon reservoir's memory of its previous state on the time scale for the evolution of the atomic system, i.e., $G(t-t')$ is the memory kernel.

We now solve Eqs. (17a) and (17b) for the amplitudes $b_{2,3}(t)$ which determine the dynamical evolution of the sys-

tem. Upon taking the Laplace transforms of Eqs. (17a) and (17b), and using the initial conditions (12a) and (12b), we find that

$$\tilde{b}_3(s)=\frac{s\cos\theta-\Omega e^{i\phi}\sin\theta}{s^2+s\tilde{G}(s)+\Omega^2}, \tag{19a}$$

$$\tilde{b}_2(s)=\frac{e^{i\phi_p}\sin\theta[s+\tilde{G}(s)]+\Omega e^{i\phi_c}\cos\theta}{s^2+s\tilde{G}(s)+\Omega^2}, \tag{19b}$$

where $\tilde{b}_{2,3}(s)$ and $\tilde{G}(s)$ are the Laplace transforms of $b_{3,2}(t)$ and $G(t)$, respectively, as defined by $\tilde{f}(s)=\int_0^\infty e^{-st}f(t)dt$, and

$$\phi=\phi_p-\phi_c \tag{20}$$

is determined by the relative phase between the control and pump lasers. For a given dispersion relation $\omega_{\mathbf{k}}$, we can calculate $G(t-t')$ from Eq. (18) which, in turn, can be used to calculate $\tilde{G}(s)$. This $\tilde{G}(s)$ can then be used in Eqs. (19a) and (19b), and the resulting expressions inverted to find analytical expressions for the amplitudes $b_{2,3}(t)$. The atomic population $n_j(t)$ of level $|j\rangle$ $(j=2,3)$ (i.e., the probability of finding the atom in level $|j\rangle$), and its steady-state value n_{js}, are then given by

$$n_j(t)\equiv|b_j(t)|^2, \quad n_{js}\equiv\lim_{t\to\infty}|b_j(t)|^2 \quad (j=2,3). \tag{21}$$

III. MODEL SYSTEM IN VACUUM

For comparison and interpretation purposes, it is instructive to first consider the case when our model system is in free space. For the free-space case, the spontaneous emission $|2\rangle\to|1\rangle$ for the V system can be ignored if $\gamma_{21}\ll\gamma_{31}$; and the spontaneous emission $|3\rangle\to|2\rangle$ for the Λ system can be ignored if $\gamma_{32}\ll\gamma_{31}$. Free space is characterized by the isotropic dispersion relation $\omega_k=ck$. For such a dispersion relation the Green's function (18) takes the form (see Appendix A)

$$G(t-t')=\gamma_{31}\delta(t-t'), \tag{22}$$

where

$$\gamma_{m1}=\frac{1}{4\pi\epsilon_o}\frac{4\omega_{m1}^3 d_{m1}^2}{3\hbar c^3} \tag{23}$$

is the spontaneous emission rate for the transition $|m\rangle\to|1\rangle$, and $\delta(t-t')$ is the Dirac delta function. Since free space is an infinitely broad photon reservoir (flat spectrum), its response should be instantaneous and the memory effect associated with spontaneous emission dynamics is infinitesimally short compared to all times of interest for the system. Interactions governed by such a delta function memory kernel are said to be Markovian [48].

From Eq. (22) we obtain $\tilde{G}(s)=\gamma_{31}$ for the Laplace transform of the Green's function, and using this in Eqs. (19a) and (19b) we obtain

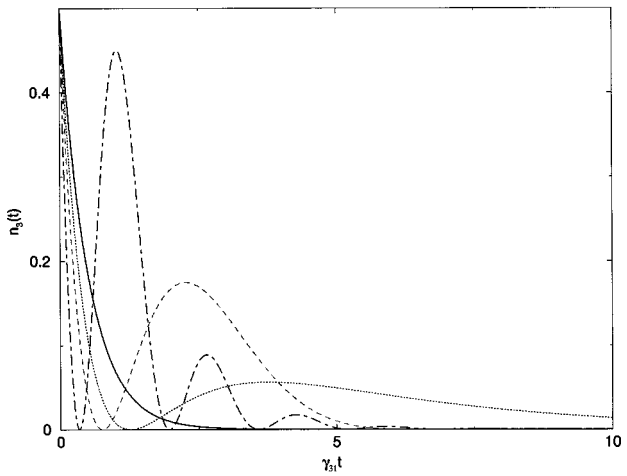

FIG. 2. Atomic population $n_3(t)$ in ordinary vacuum as a function of the scaled time $\gamma_{31}t$ for the initial conditions $\theta=\pi/4$ (that is equal superposition of the upper levels), for $\phi=-\pi/2$ and for different values of Ω, the driving field strength: $\Omega=0$ (solid curve), $\Omega=0.35\gamma_{31}$ (dotted curve), $\Omega=0.75\gamma_{31}$ (dashed curve), and $\Omega=2\gamma_{31}$ (dot-dashed curve). When $\Omega=0$ there is no transfer of population between levels $|3\rangle$ and $|2\rangle$, and therefore $n_3(t)$ exhibits simple exponential decay. Here we have assumed that spontaneous emissions on the transitions $|3\rangle\to|2\rangle$ and $|2\rangle\to|1\rangle$ are neglected either because of symmetry or because the corresponding decay rate is very small compared to γ_{31}. These results apply to both the Λ and V configurations.

$$\tilde{b}_3(s)=\frac{s\cos\theta-\Omega e^{i\phi}\sin\theta}{D(s)}, \tag{24a}$$

$$\tilde{b}_2(s)=\frac{e^{i\phi_p}\sin\theta(s+\gamma_{31})+\Omega e^{i\phi_c}\cos\theta}{D(s)}, \tag{24b}$$

where $D(s)=s^2+\gamma_{31}s+\Omega^2=(s-r_1)(s-r_2)$, with

$$r_{1,2}=-\frac{\gamma_{31}}{2}\pm\sqrt{\left(\frac{\gamma_{31}}{2}\right)^2-\Omega^2}. \tag{25}$$

Equations (24a) and (24b) are easily inverted to give

$$b_3(t)=\sum_{j=1}^{2}C_j e^{r_j t}, \quad b_2(t)=\sum_{j=1}^{2}D_j e^{r_j t}, \tag{26}$$

where

$$C_j=\frac{r_j\cos\theta-\Omega e^{i\phi}\sin\theta}{r_j-r_k} \quad (j\neq k), \tag{27a}$$

$$D_j=\frac{(r_j+\gamma_{31})e^{i\phi_p}\sin\theta+\Omega e^{i\phi_c}\cos\theta}{r_j-r_k} \quad (j\neq k). \tag{27b}$$

From Eq. (25) we see that both roots r_j are (a) negative when $\Omega\leqslant\gamma_{31}/2$; and (b) complex with a negative real part equal to $-\gamma_{31}/2$ when $\Omega>\gamma_{31}/2$. Thus the time evolution of amplitudes $b_{2,3}(t)$ [and hence of the upper level populations $n_{2,3}(t)$] can be divided into two regimes of different behavior. For $\Omega>\gamma_{31}/2$, the populations display pronounced oscillations before decaying to zero, as shown in Fig. 2, where we have plotted the atomic population $n_3(t)$ as a function of the

scaled time $\gamma_{31}t$. On the other hand, when $\Omega < \gamma_{31}/2$, the populations barely complete an oscillation before decaying to zero. When $\Omega = \gamma_{31}/2$, $D(s)=0$ has a double root $r_1 = r_2 = -\gamma_{31}/2$ and inversion of Eqs. (24a) and (24b) gives

$$b_3(t) = \{\cos\theta - [(\gamma_{31}/2)\cos\theta + \Omega e^{i\phi}\sin\theta]t\}e^{-(\gamma_{31}/2)t}, \tag{28a}$$

$$b_2(t) = e^{i\phi_p}\{\sin\theta + [(\gamma_{31}/2)\sin\theta + \Omega e^{-i\phi}\sin\theta]t\}e^{-(\gamma_{31}/2)t}. \tag{28b}$$

Thus the driving field induces oscillations on the populations of the upper levels. The stronger the driving field (i.e., the larger the Ω), the faster the oscillations.

Equation (25) shows that both roots $r_j (j=1,2)$ have a negative real part, irrespective of the value of Ω. This means that the amplitudes $b_{2,3}(t)$ decay in time and tend to zero as $t \to \infty$ so that steady state populations n_{2s} and n_{3s} are both zero:

$$n_{js} \equiv \lim_{t\to\infty} |b_j(t)|^2 = 0 \quad (j=2,3). \tag{29}$$

In other words, in free space, the populations of the excited states $|3\rangle$ and $|2\rangle$ eventually decay to the ground level $|1\rangle$ (there is no population trapped on the upper levels), independent of the strength Ω of the driving field. The only effect of the driving field is to cause transfer of populations from $|3\rangle$ to $|2\rangle$, and vice versa, until all the upper-level populations decays to the ground level. This is a general result valid for almost any broadband smoothly varying electromagnetic density of states. On the other hand, when the density of electromagnetic modes vanishes in the vicinity of an atomic transition (such as near a photonic band edge) photon localization leads to nonzero steady-state atomic populations on the excited levels [10]. The extent of localization depends sensitively on Ω and the initial atomic state, as will be seen in Sec. IV.

IV. MODEL SYSTEM IN A PBG MATERIAL

We now consider the case where our three-level system is placed within a PBG structure in such a way that the transition frequency ω_{31} is near the edge of a photonic band gap [8–10]. In a PBG one finds a modified dispersion relation for the photons in the radiation reservoir. We begin by considering an isotropic ''effective-mass'' approximation [8] for the photon dispersion relation in a PBG material:

$$\omega_{\mathbf{k}} \approx \omega_a + A(k-k_0)^2, \quad A \approx \omega_a/k_0^2 \approx c^2/\omega_c, \tag{30}$$

where ω_a is the upper band-edge frequency and k_0 is a constant characteristic of the dielectric material. This dispersion relation is valid for frequencies close to the upper photonic band edge. If the photonic band gap is large and if the relevant atomic transitions are near the upper band edge, it is a very good approximation to completely neglect the effects of the lower (dielectric) band.

The dispersion relation (30) is isotropic since it depends only on the magnitude k of the wave vector $\mathbf{k}$. While there is no physical PBG material with an isotropic gap, this provides an instructive toy model for studying quantum optical effects. Such a dispersion relation associates the band-edge wave vector with a sphere in k space, $|\mathbf{k}| = k_0$. By associating the band edge with the entire sphere $|\mathbf{k}| = k_0$ (spherical Brillouin zone), the isotropic model (30) artificially increases the true phase space available for photon propagation near the band edge. This results in a photonic density of states $\rho(\omega)$ which, near the band edge ω_a, behaves as $(\omega-\omega_a)^{-1/2}, \omega > \omega_a$, the square-root singularity being characteristic of a one-dimensional phase space [8].

In a real three-dimensional PBG material with an allowed point-group symmetry the gap is highly anisotropic and the band edge is associated with a point $\mathbf{k} = \mathbf{k}_0$ (or a finite collection of symmetry related points) in k space, rather than with the entire sphere $|\mathbf{k}| = k_0$. In other words, the magnitude of the band-edge wave vector varies as $\mathbf{k}$ is rotated throughout the Brillouin zone. Thus a more realistic picture of the band-edge behavior requires the incorporation of the Brillouin-zone anisotropy. In the effective-mass approximation, the photon-dispersion relation takes the vector form

$$\omega_{\mathbf{k}} \approx \omega_a + A(\mathbf{k}-\mathbf{k}_0)^2, \quad A \approx \omega_a/k_0^2. \tag{31}$$

This anisotropic effective-mass dispersion relation leads to a photonic density of states at a band edge ω_a which behaves as $\rho(\omega) \sim (\omega-\omega_a)^{1/2}, \omega > \omega_a$, characteristic of a three-dimensional phase space [8].

The isotropic dispersion relation (30) leads to qualitatively correct physics. However, the anisotropic model (31) introduces important quantitative corrections [8]. The most significant difference between the anisotropic and isotropic models comes out more explicitly when considering an undriven two-level atom with frequency near the edge of a photonic band gap. In this case the isotropic model leads to nonzero steady population on the upper level even when the transition frequency is slightly outside the gap [10], whereas the anisotropic model leads to fractionalized steady-state population on the upper level only when the transition frequency is inside the gap (see Appendix C).

As shown in Appendix A, under the effective-mass anisotropic dispersion relation (31), the Green's functions (18) take the form

$$G(t-t') = -\alpha \frac{e^{i[\delta(t-t')+\pi/4]}}{\sqrt{4\pi(t-t')^3}}, \quad \omega_a(t-t') \gg 1, \tag{32}$$

where

$$\alpha \approx \frac{1}{4\pi\epsilon_o}\frac{\omega_{31}^{5/2} d_{31}^2}{3\hbar c^3} \tag{33}$$

(α^2 has the dimension of frequency), and

$$\delta = \omega_{31} - \omega_a \tag{34}$$

represents the detuning of the atomic transition frequency ω_{31} from the upper band edge frequency ω_a. Equation (32) is valid only when $\omega_a(t-t') \gg 1$. The full expression for $G(t-t')$, including its short-time behavior, was given in Ref. [49]. This rather complicated general expression for $G(t-t')$ differs from the approximate expression (32) only

in the region $(t-t')\rightarrow 0_+$, which is not of much interest to us [49], as we are mainly interested in long-time memory effects.

Equation (32) shows that the memory kernel $G(t-t')$ decays with time as a power-law decay, and describes long-time memory effects in spontaneous emission dynamics due to the presence of the photonic band gap. In other words, the atom-reservoir interaction within a PBG is highly non-Markovian [49]. For the isotropic dispersion relation (30) the memory kernel $G(t-t')$ decays in times as $(t-t')^{-1/2}$ (see Appendix A). This enhanced memory for the isotropic model is an artifact of the singular phase space occupied by the band-edge photons of vanishing group velocity.

For the anisotropic band edge in the effective-mass approximation, the Laplace transform of Eq. (32) is given by

$$\tilde{G}(s)=\alpha e^{i\pi/4}\sqrt{s-i\delta}. \tag{35}$$

Using this in Eqs. (19a) and (19b), we obtain

$$\tilde{b}_3(s+i\delta)=\frac{(s+i\delta)\cos\theta-\Omega e^{i\phi}\sin\theta}{D(s)}, \tag{36a}$$

$$\tilde{b}_2(s+i\delta)=[(s+\alpha e^{i\pi/4}\sqrt{s}+i\delta)e^{i\phi_p}\sin\theta + \Omega e^{i\phi_c}\cos\theta]/D(s), \tag{36b}$$

where

$$D(s)=(s+i\delta)^2+\alpha e^{i\pi/4}(s+i\delta)\sqrt{s}+\Omega^2 =\prod_{j=1}^{4}(\sqrt{s}-e^{i\pi/4}u_j). \tag{37}$$

Here $u_j (j=1,\ldots,4)$ are the roots of the quartic equation

$$x^4+\alpha x^3+2\delta x^2+\alpha\delta x-(\Omega^2-\delta^2)=0 \tag{38}$$

given by [50]

$$u_{1,3}=-\sigma_1\pm[A-r/2+\sigma_1^2]^{1/2}, \tag{39a}$$

$$u_2=u_4^*=-\sigma_2-i[A+r/2-\sigma_2^2]^{1/2}, \tag{39b}$$

where

$$A=(r^2/4+\Omega^2-\delta^2)^{1/2}, \tag{40a}$$

$$\sigma_{1,2}=\frac{1}{4}(\alpha\pm\sqrt{\alpha^2-8\delta+4r}), \tag{40b}$$

$$r=(B-q/2)^{1/3}-(B+q/2)^{1/3}+\eta_1/3, \tag{40c}$$

$$B=\left[\left(\frac{p}{3}\right)^3+\left(\frac{q}{2}\right)^2\right]^{1/2}, \tag{40d}$$

$$p=-\frac{\eta_1^2}{3}+\eta_2,\quad q=-2\left(\frac{\eta_1}{3}\right)^3+\frac{\eta_1\eta_2}{3}+\eta_3, \tag{40e}$$

$$\eta_1=2\delta,\quad \eta_2=\alpha^2\delta+4(\Omega^2-\delta^2), \tag{40f}$$

$$\eta_3=(\alpha^2-8\delta)(\Omega^2-\delta^2)-\alpha^2\delta^2. \tag{40g}$$

Numerical analysis shows that the roots $u_{1,3}$ are real (u_1 is positive but u_2 is negative), and the roots $u_{2,4}$ are complex conjugates of each other with a negative real part (u_2 and u_4 lie in the third and second quadrants, respectively). The amplitude $b_j(t)$ is found by inverting expression (36a) for $\tilde{b}_j(s+i\delta)$ using the complex inversion formula which involves a contour integration in the complex s plane as shown in Appendix B. This gives

$$b_3(t)=\sum_{j=1}^{2}P_jQ_{3j}e^{i(u_j^2+\delta)t}+\frac{\alpha e^{i\pi/4}}{\pi}\int_0^\infty\frac{g_3(x)e^{-(x-i\delta)t}}{Z(x)}dx, \tag{41a}$$

$$b_2(t)=\sum_{j=1}^{2}P_jQ_{2j}e^{i(u_j^2+\delta)t} + \frac{\alpha\Omega e^{i(\phi_c+\pi/4)}}{\pi}\int_0^\infty\frac{g_2(x)e^{-(x-i\delta)t}}{Z(x)}dx, \tag{41b}$$

where

$$P_j=\frac{2u_j}{(u_j-u_l)(u_j-u_m)(u_j-u_n)} \quad (l,m,n=1,\ldots,4, j\neq l\neq m\neq n), \tag{42a}$$

$$Q_{3j}=(u_j^2+\delta)\cos\theta+i\Omega e^{i\phi}\sin\theta, \tag{42b}$$

$$Q_{2j}=(u_j^2+\alpha u_j+\delta)e^{i\phi_p}\sin\theta-i\Omega e^{i\phi_c}\cos\theta, \tag{42c}$$

$$g_3(x)=[(-x+i\delta)\cos\theta-\Omega e^{i\phi}\sin\theta](-x+i\delta)\sqrt{x}, \tag{42d}$$

$$g_2(x)=[(-x+i\delta)\cos\theta-\Omega e^{i\phi}\sin\theta]\sqrt{x}, \tag{42e}$$

$$Z(x)=[(-x+i\delta)^2+\Omega^2]^2+i\alpha^2(-x+i\delta)^2x. \tag{42f}$$

Since u_1 is real and u_2 is complex with negative real and imaginary parts, the first term in Eq. (41a) for the amplitude $b_3(t)$ is a nondecaying oscillatory term whereas the second term is also oscillatory but decays exponentially to zero as $t\rightarrow\infty$. The last term containing the integral represents the branch cut contribution (arising from the deformation of the contour of integration around a branch point in the complex inversion formula). This also decays to zero as $t\rightarrow\infty$, faster than the second term.

Equation (41a) shows that, as a result of the strong interaction between the atom and its own localized radiation field, level $|3\rangle$ splits into dressed-states. This dressed state splitting is the combined effect of vacuum-field Rabi splitting by the gap [51] and the Autler-Townes splitting [52] by the external field. The dressed states occur at frequencies $\omega_c-\mathrm{Im}\{iu_1^2\}=\omega_c-u_1^2$ (since u_1 is real) and $\omega_c-\mathrm{Im}\{iu_2^2\}=\omega_c-\mathrm{Re}\{u_2^2\}$. The dressed state at frequency $\omega_c-u_1^2$ lies inside the gap and is responsible for the the fractional steady-state population on the excited state. It corresponds the photon-atom bound dressed state with no decay in time. A photon emitted by an atom in such a dressed state will exhibit tunneling on a length scale given by the localization length before being Bragg reflected back to the emitting atom and

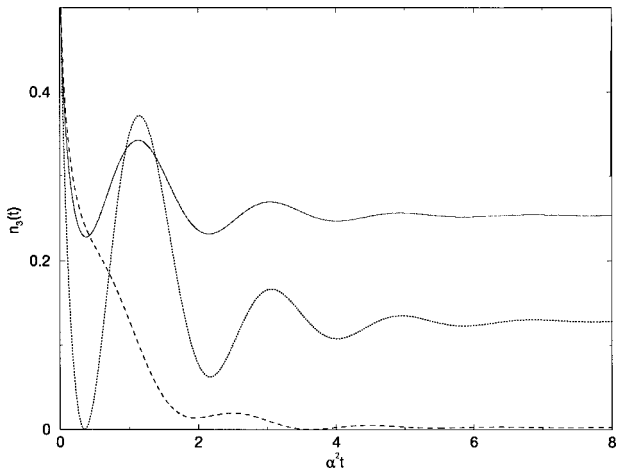

FIG. 3. Atomic population $n_3(t)$ in a PBG material as a function of the scaled time $\alpha^2 t$ for $\Omega/\alpha^2=2$, $\delta/\alpha^2=1$, and $\theta=\pi/4$, and for the relative phase $\phi=-\pi/2$ (solid curve), $\phi=0$ (dotted curve), and $\phi=\pi/2$ (dashed curve). The photon dispersion is described by the anisotropic effective-mass approximation. The steady-state population of level $|3\rangle$ is largest for the relative phase $\phi=-\pi/2$. Here we have assumed that spontaneous emissions on the transitions $|3\rangle \rightarrow |2\rangle$ and $|2\rangle \rightarrow |1\rangle$ are neglected (the leading approximation) either because of symmetry or because the transition is deep within the band gap. The figure is relevant to both Λ and V configurations.

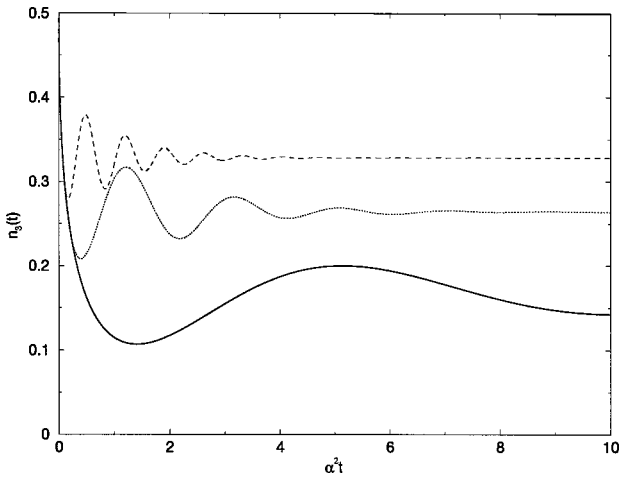

FIG. 4. Atomic population $n_3(t)$ as a function of the scaled time $\alpha^2 t$ for $\delta=0$ (i.e., when the transition $|3\rangle \rightarrow |1\rangle$ coincides with the anisotropic band edge), for the relative phase $\phi=-\pi/2$, for $\theta=\pi/4$ and $\Omega=0.5\alpha^2$ (solid curve), $\Omega=2\alpha^2$ (dotted curve), and $\Omega^2=5\alpha^2$ (dashed curve). Note that as Ω is increased, $n_3(t)$ oscillates faster, and reaches its steady-state value quicker. Moreover, the steady-state value n_{3s} increases with Ω. The results are obtained in the leading approximation, making them applicable to both the Λ and V configurations.

re-exciting it. The photon-atom bound dressed state inside the gap was predicted in Ref. [8]. The dressed state at the frequency $\omega_c - \mathrm{Re}\{u_2^2\}$ lies outside the gap (since $\mathrm{Re}\{u_2^2\} < 0$ for all $\delta > 0$) and decays at a rate of $\mathrm{Im}\{u_2^2\}$. It results in a highly non-Markovian decay of the atomic population $n_3(t)$. As ω_{31} is detuned further into the gap (i.e., as δ becomes more negative), a greater fraction of the light is localized in the gap dressed state. Conversely as ω_{31} is moved out of the gap, total emission intensity from the decaying dressed state is increased [10,49].

As a result of interference between the three terms in Eq. (41a), the spontaneous emission dynamics displays oscillatory behavior [10]. As can be seen from Eqs. (41a) and (41b), the dynamics of spontaneous emission strongly depends on the detuning $\delta=\omega_{31}-\omega_a$ of level $|3\rangle$ from the upper band edge, the initial coherent superposition state as defined by the parameter θ, the intensity Ω of the control laser driving the transition between the upper levels, and the relative phase $\phi=\phi_p-\phi_c$ between the cw control laser field and the pumping laser pulse. In Fig. 3 we plot the atomic population $n_3(t)$ as a function of the scaled time $\alpha^2 t$ for various values of the relative phase ϕ. This figure shows that, all other conditions being equal, the fractionalized steady-state population on the excited states is maximum or minimum when the relative phase is $\phi=-\pi/2$ or $\phi=\pi/2$, respectively. Figure 3 and the next three figures apply to the leading approximation of our model system whereby spontaneous emissions on the transitions $|3\rangle \rightarrow |2\rangle$ and $|2\rangle \rightarrow |1\rangle$ are neglected either because of symmetry or because the transition is deep within the band gap. All figures which are based on the leading approximation are relevant for both Λ and V configurations.

Figure 4 depicts the population $n_3(t)$ for various values of Ω. From this figure we note that, as Ω is increased, $n_3(t)$ oscillates faster and reaches its steady-state value more quickly. Moreover, the steady-state value n_{3s} increases with Ω. In the leading approximation considered in this section, single-photon spontaneous emission for the transition $|2\rangle \rightarrow |1\rangle$ is neglected for both the Λ and V configurations. This means that the population of level $|2\rangle$ cannot decay directly to level $|1\rangle$, and its only decay mechanism is indirectly through level $|3\rangle$ via the coupling Ω. When the upper levels $|3\rangle$ and $|2\rangle$ are not coupled by a control laser field ($\Omega=0$), the only decay channel of level $|2\rangle$ will be closed and the amplitude $b_2(t)$ will remain constant at its initial value $b_2(0)$ [see Eq. (17a)]. It follows that, when $\Omega=0$, our model system in the leading approximation reduces to a two-level system consisting of levels $|3\rangle$ and $|1\rangle$ with the transition frequency ω_{31} near the edge of a PBG. The dynamics of spontaneous emission by such an undriven two-level atom near the edge of an isotropic PBG was considered in detail in Ref. [10]. The effect of the anisotropy of the band edge on such an undriven two-level atom is briefly discussed in Appendix D. In Sec. V, we will show that the neglect of spontaneous emission $|2\rangle \rightarrow |1\rangle$ is a good approximation in the presence of a strong control laser field amplitude Ω. However, in the absence of the control laser field ($\Omega=0$), the spontaneous emission of a localized photon of frequency ω_{21} (inside the gap) can interfere quantum mechanically with the spontaneous emission $|3\rangle \rightarrow |1\rangle$. For a V system, this results in a nonzero steady-state population on level $|3\rangle$ even when ω_{31} is slightly above the anisotropic PBG.

In the long-time limit, only the first terms in Eqs. (41a) and (41b) remain dominant, since u_1 is real whereas u_2 is complex with a negative real part. The steady-state populations n_{js} on the upper levels $|3\rangle$ and $|2\rangle$, are thus given by

$$n_{js} \equiv \lim_{t\rightarrow\infty} |b_j(t)|^2 = |P_1 Q_{j1}|^2 \quad (j=2,3). \tag{43}$$

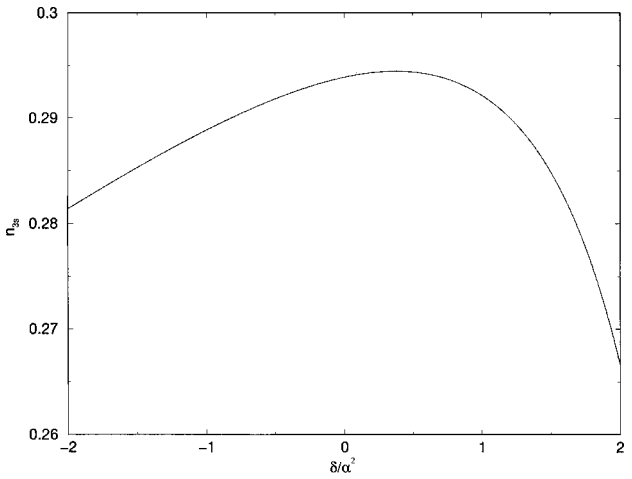

FIG. 5. Steady-state population n_{3s} of level $|3\rangle$ as a function of the detuning δ from the anisotropic 3-d band edge for $\Omega/\alpha^2=3$, $\theta=\pi/4$ and for the relative phase $\phi=-\pi/2$ [which, as seen in Fig. (3), leads to a large steady-state population]. Note that n_{3s} is nonzero outside that gap (i.e., for $\delta>0$).

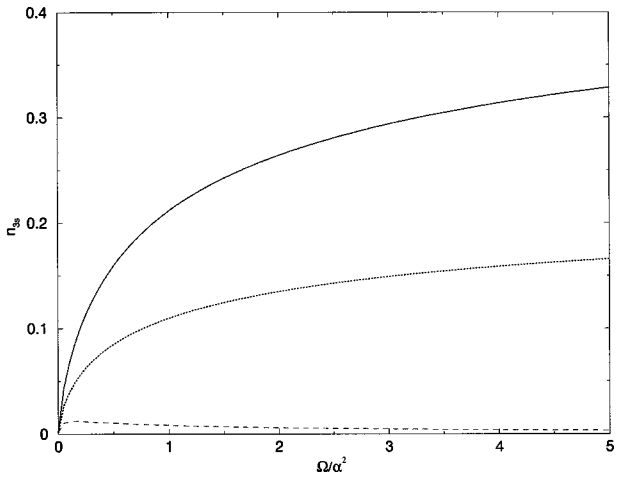

FIG. 6. Steady-state population n_{3s} of level $|3\rangle$ as a function of Ω when the transition $|3\rangle\rightarrow|1\rangle$ coincides with the anisotropic band edge ($\delta=0$). The atom is initially in a coherent superposition of the upper states $|3\rangle$ and $|2\rangle$ with $\theta=\pi/4$ and for $\phi=-\pi/2$ (solid curve), $\phi=0$ (dotted curve), and $\phi=\pi/2$ (dashed curve). n_{3s} can be an increasing or decreasing function of Ω depending on the relative phase ϕ. Results for the Λ and V configurations are the same in the leading approximation.

This phenomenon of population trapping is due to the presence of a PBG material and is absent in free space. It is apparent from Eqs. (40b)–(40f) and (42a)–(42d) that the steady-state populations n_{js} depend strongly on the parameters θ, $\phi=\phi_p-\phi_c$, $\delta=\omega_{31}-\omega_c$, and Ω. Figure 5 shows the variation of the steady-state population n_{3s} of level $|3\rangle$ with respect to the detuning δ. We see that as δ increases from zero (that is, as level $|3\rangle$ is pushed further away from the band edge into the continuum) the steady-state population n_{3s} initially increases and attains its maximum value of about 0.295 at about $\delta=0.5\alpha^2$ before it begins to decrease vary rapidly. In other words there is a fractionalized steady-state atomic population on the excited state $|3\rangle$ even when the bare excitation frequency of this level lies outside of the photonic band gap, but not far from the band edge. Remarkably, spontaneous emission is partially inhibited even within the allowed electromagnetic continuum as a consequence of quantum interference with the driving field which couples level $|3\rangle$ to the photon-atom bound state associated with level $|2\rangle$. When there is no driving field, our model system can be viewed as a two-level system consisting of levels $|3\rangle$ and $|1\rangle$, with the transitions frequency ω_{31} near the edge of a PBG. As shown in Appendix D, for such a two-level atom and the anisotropic dispersion relation (31), the steady-state population on the excited level $|3\rangle$ vanishes when the level is at the band edge or outside the gap. However, population trapping in a V system, on level $|3\rangle$ outside the PBG, in the absence of a control laser field, may be recaptured by going beyond the leading approximation and including the spontaneous emission channel $|2\rangle\rightarrow|1\rangle$.

Figure 6 depicts the variation of n_{3s} with respect of the strength Ω of the driving field for various values of the relative phase ϕ. This figure shows that n_{3s} can be an increasing or decreasing function of Ω depending on the value of the relative phase ϕ. For a very strong control laser field (that is, when $\Omega\gg\alpha^2,\delta$) the steady-state populations n_{js} are given approximately (see Appendix B) by

$$n_{3s}\approx n_{2s}\approx\tfrac{1}{4}(1-\sin 2\theta\sin\phi). \tag{44}$$

Equation (44) shows that, when $\theta=0$ or $\theta=\pi/2$ (i.e., when the atom is initially on level $|3\rangle$ or on level $|2\rangle$), we have $n_{3s}=n_{2s}=1/4$. In other words, for the case of a strong laser field, the steady-state atomic populations n_{3s} and n_{2s} are independent of the initial relative phase ϕ when $\theta=0$ or $\theta=\pi/2$ (if the system is not initially prepared as a coherent superposition of the upper states). However, if the atom is initially prepared in a coherent superposition of the two upper states $|3\rangle$ and $|2\rangle$, so that $\sin(2\theta)\neq 0$ in Eq. (44), the steady-state atomic populations will also depend on ϕ . For instance when $\theta=\pi/4$, spontaneous emission is strongly enhanced ($n_{3s}+n_{2s}\approx 0$) for $\phi=\pi/2$, whereas it is totally suppressed ($n_{3s}+n_{2s}\approx 1$) for $\phi=-\pi/2$. Clearly, the steady-state atomic population keeps a memory of the initial relative phase ϕ. It can be controlled by changing the optical paths of the pumping and controlling lasers. Moreover, due to the effects of photon localization, the atom keeps a memory of the intensity and phase of the pump (input) laser pulse. This suggests that our model system can serve as an optical memory device on the atomic scale.

An important consideration in applications such as quantum computing is the coherence of the atomic amplitudes in the steady-state limit. In the leading approximation, it is easy to verify that the off-diagonal elements of the atomic density matrix retain their coherence in the long-time limit. Equations (41a) shows that in the steady-state limit the cross-term $b_3(t)b_2^*(t)$ is given by

$$\lim_{t\rightarrow\infty} b_3(t)b_2^*(t)=|P_1|^2Q_{31}Q_{21}^*, \tag{45}$$

and for a very strong control laser field ($\Omega\gg\alpha^2,\delta$) this reduces to (see Appendix B)

$$\lim_{t\rightarrow\infty} b_3(t)b_2^*(t)\approx\frac{ie^{-i\phi_c}}{4}(1-\sin 2\theta\sin\phi). \tag{46}$$

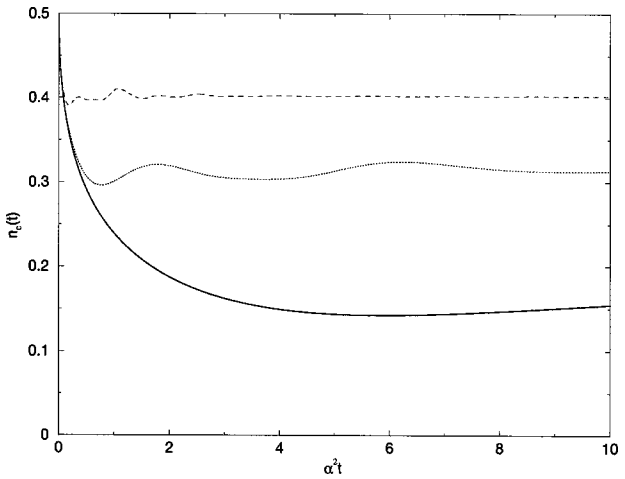

FIG. 7. The coherence $n_c(t)=|b_3(t)b_2^*(t)|$ between levels $|3\rangle$ and $|2\rangle$ in the leading approximation for ω_{31} tuned to the anisotropic band edge ($\delta=0$) as a function of the scaled time $\alpha^2 t$ for $\Omega=0.1\alpha^2$ (solid curve), $\Omega=\alpha^2$ (dotted curve), and $\Omega=5\alpha^2$ (dashed curve). The atom is initially in a coherent superposition of the upper states $|3\rangle$ and $|2\rangle$ with $\theta=\pi/4$ and $\phi=-\pi/2$. Results apply to both Λ and V systems.

Thus not only do the upper levels $|3\rangle$ and $|2\rangle$ have nonzero populations (n_{2s} and n_{3s}) in the steady-state limit, as required for a classical memory device, but the coherences are nonzero in the steady-state limit as required for quantum memory. In essence, coherence is forced on the atomic system by means of the external laser field. Like the populations $n_{2,3}(t)$, the coherence $n_c(t)=|b_3(t)b_2^*(t)|$ depends strongly on the parameters θ, $\phi=\phi_p-\phi_c$, $\delta=\omega_{31}-\omega_a$ and Ω. Equation (46) shows that for large Ω, and when the system is initially prepared in a coherent superposition of the upper states (i.e., when $\theta\neq 0$ and $\pi/2$), the coherence $n_c(t)$ between levels $|3\rangle$ and $|2\rangle$ can be controlled by the relative phase ϕ, and attains its maximum value when $\phi=-\pi/2$. In Fig. 7 we plot the coherence $n_c(t)$ as a function of the scaled time $\alpha^2 t$ for different values of Ω. We see that, for the chosen conditions, $n_c(t)$ increases with increasing Ω. In Secs. V and VI, we discuss how the coherence $n_c(t)$ is influenced by other spontaneous emission and nonradiative effects that are not considered within the leading approximation.

All the above results for the anisotropic model (31) are qualitatively similar to those derived for the isotropic model (30). In particular, exactly the same relation as Eq. (44) holds for the isotropic model (30) [53]. The major difference between the two dispersion models is that the time-scale factor for the transient radiative dynamics is α^{-2} [where α is given by Eq. (33)] for the anisotropic model, whereas it is β^{-1} [where β is given by Eq. (A19)] for the isotropic model.

The above considerations suggest that quantum information can be ''written'' onto a single three-level atom by choosing the ''area'' of the incident laser pulse, the intensity of the cw laser, and the relative optical path lengths of the cw and pulse-laser beams. In other words, the precise nature of the information written onto the quantum bit or ''qubit'' can be controllably altered by varying these external parameters. Furthermore, the phase and intensity of the control laser field can be adjusted so that spontaneous emission can be totally suppressed in our model system. That is to say, at steady state, the system can be in a coherent superposition of the upper states $|3\rangle$ and $|2\rangle$ as $|\phi\rangle=a_3|3\rangle+a_2|2\rangle$ with $|a_3|^2+|a_2|^2=1$, the amplitudes a_2 and a_3 being dependent on the phase and intensity of the pump laser pulse. Since this superposition state is immune to single-photon radiative decay, it is a promising candidate for a two-level quantum bit to encode information in quantum computations. In Secs. V and VI we discuss some possible decoherence mechanisms. This is the greatest obstacle to quantum computation since it causes a pure quantum state to evolve into a mixture of states, and to thereby lose two of its key properties: interference and entanglement [54].

V. EFFECTS OF OTHER SPONTANEOUS EMISSION TERMS

In the leading approximation for our model system of Fig. 1, we have assumed that spontaneous emission on the transitions $|3\rangle\rightarrow|2\rangle$ and $|2\rangle\rightarrow|1\rangle$ is inhibited, either by symmetry consideration or by the presence of the PBG. We next relax this assumption to see its effects on the system dynamics. To this end we consider the V configuration of Fig. 1(b) where the upper levels $|2\rangle$ and $|3\rangle$ are of the same symmetry and are both coupled by dipole transitions to the ground level $|1\rangle$. In this case the unperturbed Hamiltonian H_0 is still the same as that of Eq. (7) whereas H_I has an additional term due to the allowed $|2\rangle\rightarrow|1\rangle$ transition. It is given by

$$H_I=i\hbar\Omega[e^{i(\omega_L t+\phi_c)}\sigma_{23}-e^{-i(\omega_L t+\phi_c)}\sigma_{32}]+i\hbar\sum_{\mathbf{k}\lambda}[g_{\mathbf{k}\lambda}^{31}(a_{\mathbf{k}\lambda}^{\dagger}\sigma_{13}-\sigma_{31}a_{\mathbf{k}\lambda})+g_{\mathbf{k}\lambda}^{21}(a_{\mathbf{k}\lambda}^{\dagger}\sigma_{12}-\sigma_{21}a_{\mathbf{k}\lambda})], \quad (47)$$

where

$$g_{\mathbf{k}\lambda}^{i1}=\frac{\omega_{i1}d_{i1}}{\hbar}\left(\frac{\hbar}{2\epsilon_o\omega_{\mathbf{k}}V}\right)^{1/2}\hat{\mathbf{e}}_{\mathbf{k}\lambda}\cdot\hat{\mathbf{d}}_{i1}\quad(i=2,3), \quad (48)$$

the coupling constant between the atomic transition $|i\rangle\rightarrow|1\rangle$ and the mode $\{\mathbf{k}\lambda\}$ of the radiation field. With this interaction Hamiltonian, Eqs. (14) are replaced by

$$\dot{b}_{1\mathbf{k}\lambda}(t)=g_{\mathbf{k}\lambda}^{31}b_3(t)e^{i\mu_{\mathbf{k}}^{31}}+g_{\mathbf{k}\lambda}^{21}b_2(t)e^{i\mu_{\mathbf{k}}^{21}}, \quad (49a)$$

$$\dot{b}_2(t)=\Omega e^{i\phi_c}b_3(t)-\sum_{\mathbf{k}\lambda}g_{\mathbf{k}\lambda}^{21}b_{1\mathbf{k}\lambda}(t)e^{-i\mu_{\mathbf{k}}^{21}t}, \quad (49b)$$

$$\dot{b}_3(t)=-\Omega e^{-i\phi_c}b_2(t)-\sum_{\mathbf{k}\lambda}g_{\mathbf{k}\lambda}^{31}b_{1\mathbf{k}\lambda}(t)e^{-i\mu_{\mathbf{k}}^{31}t}, \quad (49c)$$

where $\mu_{\mathbf{k}}^{ij}=\omega_{\mathbf{k}}-\omega_{ij}$ is the detuning of the radiation mode frequency $\omega_{\mathbf{k}}$ from the atomic transition frequency ω_{ij}.

Formal integration (in time) of Eq. (49a) with the initial condition $b_{1\mathbf{k}\lambda}(0)=0$ yields

$$b_{1\mathbf{k}\lambda}(t)=g_{\mathbf{k}\lambda}^{31}\int_0^t b_3(t')e^{i\mu_{\mathbf{k}}^{31}t'}dt'+g_{\mathbf{k}\lambda}^{21}\int_0^t b_2(t')e^{i\mu_{\mathbf{k}}^{21}t'}dt'. \quad (50)$$

Substituting this expression in Eqs. (49b) and (49c) gives

$$\dot{b}_2(t)=\Omega e^{i\phi_c}b_3(t)-\int_0^t G_{22}(t-t')b_2(t')dt' - e^{-i\omega_{32}t}\int_0^t G_{23}(t-t')b_3(t')dt', \quad (51a)$$

$$\dot{b}_3(t)=-\Omega e^{-i\phi_c}b_2(t)-\int_0^t G_{33}(t-t')b_3(t')dt' - e^{i\omega_{32}t}\int_0^t G_{32}(t-t')b_2(t')dt', \quad (51b)$$

where

$$G_{ij}(t-t')=\sum_{\mathbf{k}\lambda} g_{\mathbf{k}}^{i1}g_{\mathbf{k}\lambda}^{j1}e^{-i\mu_{\mathbf{k}\lambda}^{j1}(t-t')} \quad (i,j=2,3) \quad (52)$$

are the delay Green's functions. Equations (51a) and (51b) are the generalized versions of Eqs. (17a) and (17b) for a V system including spontaneous emission on the transition $|2\rangle\rightarrow|1\rangle$. We will next solve these generalized equations for the amplitudes $b_3(t)$ and $b_2(t)$. In order to explicitly see the effects of the control laser driving the transition $|3\rangle\rightarrow|2\rangle$ on the system dynamics, we consider the cases $\Omega=0$ and $\Omega\neq 0$ separately. The $\Omega=0$ (quantum beats) case is a valuable reference case for interpreting the results of the $\Omega\neq 0$ (coherent control) case. For each of the above cases, we consider both the system in vacuum and the system in a PBG.

A. System in vacuum

For the free space dispersion relation $\omega_k=ck$, the Green's functions (52) take the form (see Appendix A)

$$G_{ij}(t-t')=\eta_{ij}\sqrt{\gamma_{i1}\gamma_{j1}}\delta(t-t') \quad (i,j=2,3), \quad (53)$$

where γ_{m1} is the spontaneous emission rate for the transition $|m\rangle\rightarrow|1\rangle$ given by Eq. (23), $\delta(t-t')$ is the Dirac delta function, and

$$\eta_{ij}=\delta_{ij}+\eta(1-\delta_{ij}) \quad (i,j=2,3). \quad (54)$$

Here δ_{ij} is the Krönecker delta function and η is a constant (defined in Appendix A), which satisfies $|\eta|\leqslant 1$, the equality sign holding when the dipoles associated with the transitions $|i\rangle\rightarrow|1\rangle$ and $|j\rangle\rightarrow|1\rangle$ are parallel or antiparallel (when $\hat{\mathbf{d}}_{i1}=\pm\hat{\mathbf{d}}_{j1}$). With the free-space forms [Eq. (53)] of the Green's functions, the general equations (51a) and (51b) reduce to

$$\dot{b}_2(t)=-\gamma_{21}b_2(t)+[\Omega e^{i\phi_c}-\eta\bar{\gamma}e^{-i\omega_{32}t}]b_3(t), \quad (55a)$$

$$\dot{b}_3(t)=-\gamma_{31}b_3(t)-[\Omega e^{-i\phi_c}+\eta\bar{\gamma}e^{i\omega_{32}t}]b_2(t), \quad (55b)$$

where

$$\bar{\gamma}=\sqrt{\gamma_{21}\gamma_{31}}. \quad (56)$$

If we neglect spontaneous emission on the transition $|2\rangle\rightarrow|1\rangle$ so that both γ_{21} and η are zero, Eqs. (55a)–(55b) reduce to Eqs. (17a) and (17b), when we use Eq. (53).

1. Quantum beats in vacuum

The problem of quantum beats in vacuum corresponds to the case when $\Omega=0$ in Eqs. (55a) and (55b). This problem was considered in detail by Zhu *et al.* [55] for the case $\eta=1$, i.e., when the dipole moments of the two allowed transitions are parallel (or antiparallel). Our general model recaptures these specialized results. When $\Omega=0$, Eqs. (55a) and (55b) are easily solved to give

$$b_3(t)=e^{-\gamma_{31}t}\sum_{j=1}^{2}A_j e^{q_j t}, \quad (57a)$$

$$b_2(t)=e^{-(\gamma_{31}+i\omega_{32})t}\sum_{j=1}^{2}B_j e^{q_j t}, \quad (57b)$$

where

$$q_{1,2}=\frac{\lambda}{2}\pm\sqrt{\left(\frac{\lambda}{2}\right)^2+(\eta\bar{\gamma})^2}, \quad (58a)$$

$$\lambda=\gamma_{31}-\gamma_{21}+i\omega_{32}, \quad (58b)$$

$$A_j=\frac{q_k b_3(0)+\eta\bar{\gamma}b_2(0)}{q_k-q_j} \quad (k\neq j), \quad (58c)$$

$$B_j=-\frac{q_j A_j}{\eta\bar{\gamma}}. \quad (58d)$$

When $\eta=0$ (and $\Omega=0$), Eqs. (55a) and (55b) have simple exponentially decaying solutions $b_3(t)=b_3(0)e^{-\gamma_{31}t}$ and $b_2(t)=b_2(0)e^{-\gamma_{31}t}$. Comparing these solutions with the general solutions Eqs. (57a) and (57b) we see that, for $\eta=0$, $A_1=0$, $A_2=b_3(0)$, $B_1=b_2(0)$, and $B_2=0$.

It can easily be shown that the amplitudes $b_j(t)$ given by Eq. (57a) satisfy $\lim_{t\rightarrow\infty}b_j(t)=0$. As a result of quantum interference between the two decay channels ($|3\rangle\rightarrow|1\rangle$ and $|2\rangle\rightarrow|1\rangle$) which are coupled by the same vacuum modes, the decays of the populations $n_2(t)$ and $n_3(t)$ are not purely exponential and may display oscillatory behavior depending on the initial coherent superposition state defined by $b_3(0)$ and $b_2(0)$, on the decay rates γ_{21} and γ_{31}, and on the frequency separation ω_{32} between the two upper levels [55]. If, for instance, the system is initially prepared in the state $|\Psi(0)\rangle=|3\rangle$, then, in the course of time, the population of level $|2\rangle$ increases from zero to a maximum and then decreases to zero, while that of level $|3\rangle$ monotonically decreases to zero.

The detected signal resulting from spontaneous emission from the three-level system is proportional to

$$\mathcal{J}(t)=\left|\sum_{\mathbf{k}\lambda} b_{1\mathbf{k}\lambda}(t)\exp\{i[\mathbf{k}\cdot\mathbf{r}-(\omega_{\mathbf{k}}+\omega_1)t]\}\right|^2, \quad (59)$$

where $\mathbf{r}$ is the the position of the detector relative to the emitting atom [48]. According to Eq. (50), this has contribu-

tions from $b_2(t')$ and $b_3(t')(0 \leqslant t' \leqslant t)$ which will, in general, interfere with each other. The temporal interference of the two possible transitions $|3\rangle \rightarrow |1\rangle$ and $|2\rangle \rightarrow |1\rangle$ gives rise to a fluorescence signal that has a component modulated at the difference frequency ω_{32}. This is the phenomenon of quantum beats and is the basis of a spectroscopic technique used to determine the difference in frequency between two atomic levels [48]. When $\eta = 0$, no quantum beats are observed [48] if either $b_2(0)$ or $b_3(0)$ vanishes (i.e., if the system is not initially prepared in a coherent superposition of the upper states). However quantum beats do indeed occur when $\eta \neq 0$, even if either $b_2(0)$ or $b_3(0)$ is zero. The interference between the two possible transitions accounts for the dark line in the spontaneous emission spectrum of a three level atom in the V configuration observed in Ref. [55]. In the absence of interference between the two spontaneous emission decay processes, one expects the spectrum of the three-level atom to consist of two Lorentzian distributions peaked at the two transitions frequencies. Instead what is obtained is a single distribution with a dark band, whose width depends on the decay rates γ_{21} and γ_{31}.

A coherently excited three level atom in the V configuration can decay via the emission of a photon of frequency ω_{31} or ω_{21}. However, since both transitions lead to the same final atomic state, one cannot determine along which radiative paths ($|3\rangle \rightarrow |1\rangle$ or $|2\rangle \rightarrow |1\rangle$) the atom decay. This uncertainty in the radiative trajectory leads to interference of transition amplitudes which can be observed as quantum beats. This process is analogous to Young's double-slit experiment, where interference takes place because we are unable to distinguish between the different photon paths that lead to the detector. On the other hand, a coherently excited atom in the Λ configuration will also decay along the radiative path ω_{31} or ω_{32}. However, since the two emission path ways lead to different final states, a measurement of the final state of the atom would tell us which decay channel was taken. Consequently, no beats are expected in this case [48]. The situation would, of course, be different in the presence of a driving field coupling levels $|3\rangle$ and $|2\rangle$.

2. Coherent control in vacuum

When $\Omega \neq 0$, Eqs. (55a) and (55b) correspond to the problem of coherent control in ordinary vacuum. In this case the equations must, in general, be solved numerically. In the special case when both γ_{21} and η are set to zero, Eqs. (55a) and (55b) reduce to Eqs. (17a) and (17b), which, in turn, can be solved analytically, as shown in Sec. III. In both the coherent control case and the quantum beat case, the population dynamics depends on the initial coherent superposition state (i.e., on θ and ϕ_p) as well as on the parameters γ_{21}, γ_{31}, and ω_{32}. In the coherent control case, the atomic population has an additional dependence on the intensity Ω and phase ϕ_c of the control laser field. Just as in the case when $\gamma_{21} = 0$, the driving field causes transfer of populations from $|3\rangle$ to $|2\rangle$. The stronger the driving field, the higher the frequency of oscillation of the populations $n_{2,3}(t)$. For free space, the steady-state atomic populations on the upper levels are zero, irrespective of the control laser field amplitude Ω.

B. System in a PBG material

For the anisotropic effective-mass dispersion relation (31), the Green's functions (52) take the form (see Appendix A)

$$G_{ij}(t-t') = -\eta_{ij}\alpha \frac{e^{i[\delta_{j1}(t-t')+\pi/4]}}{\sqrt{\pi(t-t')^3}} \quad \omega_a(t-t') \gg 1, \tag{60}$$

where η_{ij} and α^2 are given, respectively, by Eqs. (54) and (33); and

$$\delta_{ij} = \omega_{ij} - \omega_a \tag{61}$$

is the detuning of the atomic transition frequency ω_{ij} from the upper band-edge frequency ω_a. Substituting Eqs. (60) into Eqs. (49a) and (49b), we can find the coupled equations for the amplitudes $b_{2,3}(t)$ appropriate for a PBG analogous to Eqs. (55a) and (55b) for vacuum. However, in the PBG case, it is convenient to introduce the new amplitudes $h_{2,3}(t)$:

$$b_j(t) = h_j(t)e^{i\delta_{j1}t} \quad (j = 2,3) \tag{62}$$

In terms of these new amplitudes and the Green's functions (60), Eqs. (49a) and (49b) can be rewritten as

$$\frac{d}{dt}h_2(t) = -i\delta_{21}h_2(t) + \Omega e^{i(\omega_{32}t+\phi_c)}h_3(t) - \int_0^t G(t-t')[h_2(t') + \eta h_3(t')]dt', \tag{63a}$$

$$\frac{d}{dt}h_3(t) = -i\delta_{31}h_3(t) - \Omega e^{-i(\omega_{32}t+\phi_c)}h_2(t) - \int_0^t G(t-t')[h_3(t') + \eta h_2(t')]dt', \tag{63b}$$

where

$$G(t-t') = -\alpha e^{i\pi/4}/\sqrt{4\pi(t-t')^3}. \tag{64}$$

We now discuss Eqs. (63) for the cases $\Omega = 0$ and $\Omega \neq 0$ separately.

1. Quantum beats near the edge of a PBG

The problem of quantum beats near the edge of a photonic band gap corresponds to the case when $\Omega = 0$ in Eqs. (63a) and (63b). This case has also been investigated in Ref. [56], using the ''effective-mass'' isotropic dispersion model (30). In this paper we will discuss the problem using the more realistic anisotropic dispersion model (31).

When $\Omega = 0$, Eqs. (63a) and (63b) can be solved to give closed analytic expressions for the amplitudes $h_{2,3}(t)$. These expressions take particularly simple forms when the band edge ω_a is midway between the two upper of levels of the V system so that $\delta_{31} = -\delta_{21} = \delta$ (thus $\delta \geqslant 0$), and when the atomic dipoles associated with the transitions $|3\rangle \rightarrow |1\rangle$ and $|2\rangle \rightarrow |1\rangle$ are parallel (or antiparallel) so that $\eta = 1$. In this special case the solutions to Eqs. (63a) and (63b) are given by (see Appendix C)

$$b_3(t)=\sum_{j=1}^{2} E_j F_{3j} e^{i(\nu_j^2+\delta)t}+\frac{e^{i\pi/4}}{\pi}\int_0^\infty \frac{f_3(x)e^{-(x-i\delta)t}dx}{W(x)}, \tag{65a}$$

$$b_2(t)=\sum_{j=1}^{2} E_j F_{2j} e^{i(\nu_j^2-\delta)t}+\frac{e^{i\pi/4}}{\pi}\int_0^\infty \frac{f_2(x)e^{-(x+i\delta)t}dx}{W(x)}, \tag{65b}$$

where $E_j, \nu_j (j=1,2)$ are constants which depend on α^2 and the detuning parameter δ. The constants F_{ij} depend on the initial coherent superposition state [as defined by the initial values $b_2(0)$ and $b_3(0)$] and on both α^2 and δ. The constant ν_1 is real, while ν_2 is a complex number with negative real and imaginary parts.

Solutions (65a) and (65b) for the amplitudes $b_{2,3}(t)$ show that (a) the spontaneous emission is oscillatory and (b) each of the upper levels splits into dressed states analogous to vacuum-field Rabi splitting in a high-Q cavity [51]. The splitting is solely due to the interaction of the atom with the photon reservoir, since there is no driving field. Furthermore, (c) there is a fractionalized steady-state population on each of the upper levels as a result of the localization of light in the vicinity of the emitting atom and (d) quantum interference leads to nonzero steady state population on level $|3\rangle$ even when it lies outside the PBG (but not far from the band edge). This reveals an important distinction between the realistic anisotropic PBG model and the isotropic dispersion model [56]. In the anisotropic model, spontaneous emission from level $|3\rangle$ (outside of the PBG) can be inhibited by quantum interference with level $|2\rangle$ (inside the PBG). This inhibition does not occur in the absence of the coupling to level $|2\rangle$. In the isotropic model, inhibition of spontaneous emission from level $|3\rangle$ occurs even in the absence of coupling to level $|2\rangle$.

In Fig. 8 we plot, using expressions (65a) and (65b), the atomic populations $n_{2,3}(t)$ as functions of the scaled time $\alpha^2 t$ assuming that, initially, the atom was on level $|3\rangle$ (i.e., $\theta=0$). As a result of quantum interference between the two allowed transitions, the population of level $|2\rangle$ (which was initially zero) increases form zero to a maximum before it settles down to a steady-state value. Similar oscillations occur in free space quantum beats [Eqs. (57a) and (57b)]. The major difference is the nonzero steady state populations in the PBG case. These steady-state populations are given by

$$n_{js}=\lim_{t\to\infty}|b_j(t)|^2=|E_1F_{j1}|^2 \quad (j=2,3), \tag{66}$$

and depend on the parameters θ, ϕ, and δ.

In order to see the detailed differences between the isotropic and anisotropic model dispersion relations [Eqs. (30) and (31), respectively], we investigated the dynamics of the populations $n_{2,3}(t)$ in the PBG quantum beats problem for the isotropic dispersion model, assuming that the atom was initially on level $|3\rangle$. Apart from the difference in time scales, the main distinction between the two models is that interference of spontaneous emission between the two allowed transitions and the localization effects of the photonic band gap are considerably enhanced for the isotropic model relative to the anisotropic model. In the isotropic model, the populations oscillate for hundreds of cycles before decaying to their final larger steady-state values. The amplitudes of these oscillations depend on the initial values $b_3(0)$ and $b_2(0)$. As mentioned in Sec. IV, this enhancement is an artifact of the singular photon density of states at the isotropic band edge.

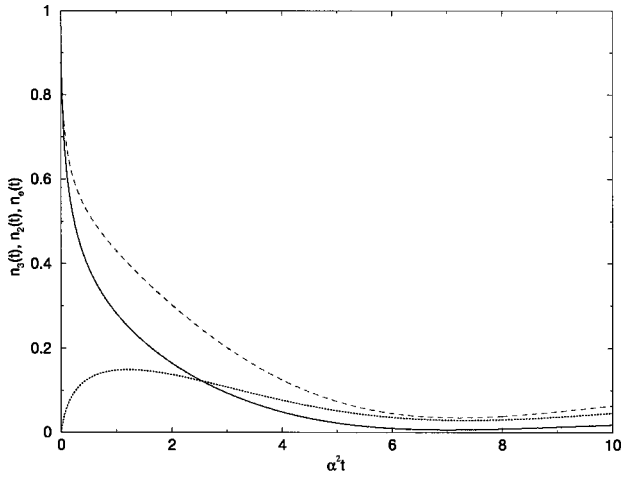

FIG. 8. V-system atomic populations $n_3(t)$ (solid curve), $n_2(t)$ (dotted curve), and the total excited-state population $n_e(t)=n_2(t)+n_3(t)$ (dashed curve) as functions of the scaled time $\alpha^2 t$ in the PBG quantum beats problem ($\Omega=0$) for the initial condition $\theta=0$ (i.e., the atom initially on level $|3\rangle$) and for $\phi=-\pi/2$ and $\eta=1$. The anisotropic band edge is midway between the two upper levels with detuning $\delta_{31}=-\delta_{21}=0.5\alpha^2$. Note that, as a result of quantum interference between the two allowed transitions, the population of level $|2\rangle$ (which was initially zero) increases form zero to a maximum before it settles down to a steady-state value of about 0.05 unlike ordinary vacuum.

2. Coherent control near the edge of a PBG

When $\Omega\neq 0$, Eqs. (63a) and (63b) correspond to the problem of coherent control near the edge of a PBG. In this case the equations do not have simple analytic solutions. They must be solved numerically. For illustration purpose it is simpler to use the isotropic rather than the anisotropic model. The Green's function $G_{lm}(t-t')$ of the isotropic model [Eq. (A18)] exhibits an integrable square root singularity [57] at $t=t'$ whereas the complete Green's function in the anisotropic model, which also has an integrable square-root singularity at $t=t'$, is rather cumbersome [49].

Figure 9 depicts the PBG coherent control problem for the isotropic dispersion model [Eq. (30)], with the additional spontaneous emission effects included. Note that, for $\Omega\neq 0$, $n_3(t)$ displays rapid oscillations within a relatively slowly varying envelope. When $\Omega\neq 0$, there are two causes for the oscillations of $n_3(t)$. The first one (slow oscillations) is the quantum interference between the two allowed transitions ($|3\rangle\to|1\rangle$ and $|2\rangle\to|1\rangle$) as in the quantum beat problem. Superimposed on this is the exchange of populations between levels $|3\rangle$ and $|2\rangle$ caused by the driving field (rapid oscillations). As Ω increases the amplitude of the envelope oscillations decreases but the frequency of the oscillations within the envelope increases. Moreover, the steady-state value n_{3s} increases with Ω. In fact for large Ω, $n_3(t)$ changes little from its initial value $n_3(0)$ even though ω_{31} lies slightly outside the gap ($\delta_{31}=0.5\beta$). This is because,

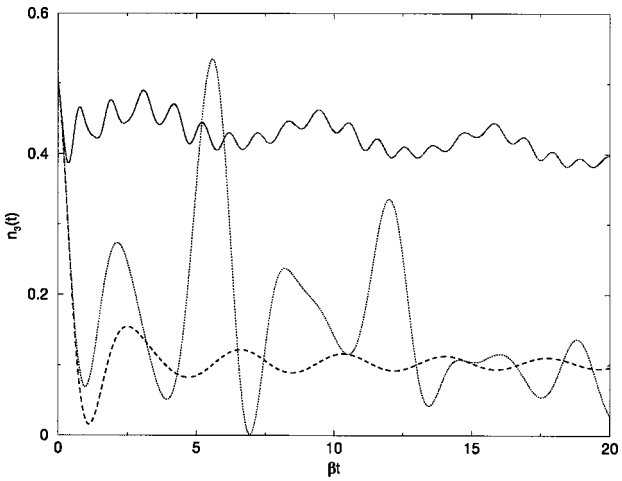

FIG. 9. V-system atomic population $n_3(t)$ as a function of the scaled time βt in the PBG (including spontaneous emission channels which go beyond the leading approximation) for $\theta=\pi/4$ and $\phi=-\pi/2$, and $\Omega=0$ (dashed curve), $\Omega=0.5\beta$ (dotted curve), and $\Omega=5\beta$ (solid curve). The isotropic band edge is midway between the two upper levels with detuning $\delta_{31}=-\delta_{21}=0.5\beta$ and $\eta=1$. For $\Omega\neq 0$, $n_3(t)$ displays rapid oscillations within a slowly varying envelope—the frequency of the oscillations within the envelope increasing with Ω.

when Ω is large, level $|3\rangle$ will be strongly coupled to level $|2\rangle$ which lies inside the gap ($\delta_{21}=-0.5\beta$).

Just as in the case of the populations $n_{2,3}(t)$, the spontaneous emission channel $|2\rangle\rightarrow|1\rangle$ introduces further oscillations to the coherence $n_c(t)$ over and above those induced by the driving field. Nevertheless we obtain nonzero steady-state coherences (and populations) as long as level $|3\rangle$ is not detuned far outside the gap. These results are qualitatively similar to those in Sec. IV, where spontaneous emission on the transition $|2\rangle\rightarrow|1\rangle$ is neglected. The incorporation of the decay channel $|2\rangle\rightarrow|1\rangle$, together with the use of the isotropic dispersion relation, leads to additional oscillations in the transient dynamics. However, it does not alter the presence of nonzero steady-state populations and coherences on the upper levels, nor does it alter the ability to control these steady-state populations and coherences by the intensity and phase of the driving field.

VI. HIGHER-ORDER RADIATIVE AND NONRADIATIVE INTERACTIONS

As discussed in Sec. IV, an excited atom in a PBG interacts strongly with its own radiation field, leading to the formation of the photon-atom bound state [8] in which the photon emitted by the excited atom can tunnel through the dielectric host on a length scale given by the localization length $\xi_{\rm loc}$ before being Bragg reflected back to the emitting atom. The result is a stationary state superposition of a localized photon and a partially excited atom as manifested by the nonzero fractionalized steady state population given by Eqs. (43) and (66).

Inside a PBG, single-photon spontaneous emission is inhibited. Thus the photon-atom bound state can decay only by other relaxation mechanisms. One such a mechanism is spontaneous two photon emission. This may be relevant for the case of a cold atom which has been optically trapped in the void regions of the PBG material, and which is not in mechanical contact with the vibrational degrees of freedom of the dielectric host. For a dipole allowed transition such as the $|2\rangle\rightarrow|1\rangle$ transition in a V system [Fig. 1(a)], two-photon decay yields a lifetime for the photon-atom bound state on the scale of days [8] if the transition lies in the visible spectrum. On the other hand, for a dipole-forbidden transition such as the the $|2\rangle\rightarrow|1\rangle$ in the Λ configuration [Fig. 1(b)], two-photon emission may occur by means of a pair of dipole transitions which occurs considerably faster. For instance the $2s\rightarrow 1s$ transition in hydrogen occurs in 1/7 seconds.

For a vapor of cold atoms trapped in a PBG, the presence of many atoms within a cubic wavelength may significantly alter the simple picture, described above, of a single photon-atom bound state. An important alteration arises from photon-hopping conduction [12,8] between impurity atoms inside a PBG via resonant dipole-dipole interaction (RDDI). For a band gap to center frequency ratio of $\Delta\omega/\omega_o\sim 5\%$, the localization length $\xi_{\rm loc}$ associated with a photonic bound state is on the scale of several optical wavelengths [8]. Thus the photon can tunnel through the dielectric host and be absorbed by another atom located within $\xi_{\rm loc}$. For atoms separated by a distance less than the optical wavelength, the photon hopping conduction occurs by means of the exchange of a high-energy virtual photons between the atoms. In this manner a single excitation can hop from one impurity atom to another. Unlike an ordinary vacuum, where RDDI effects are commonly associated with van der Waals dephasing, in a PBG material RDDI may lead to coherent transfer of excitation energy from one atom to the next. The dynamical properties of coherent RDDI-mediated photon-hopping conduction between impurity atoms inside a PBG were considered in detail in Ref. [12]. When many photons are injected into a system of atoms interacting by RDDI in a photonic band gap, highly entangled and nonclassical states of light can be formed [58]. These quantum many-body states differ significantly from the well-known symmetrical (Dicke) superradiant states in which cooperative light emission occurs at an enhanced rate in ordinary vacuum. For certain non-Dicke-type states, cooperative emission can be significantly retarded rather than enhanced. These entangled states which arise from photon-hopping conduction between impurity atoms may exhibit considerable immunity from conventional radiative or nonradiative decay mechanisms.

The effect of a photonic band gap is to simply eliminate the amplitude for single-photon, single-atom spontaneous emission. This does not exclude nonlinear decay processes. An excited impurity atom within a PBG may decay to the ground state if there is another excited impurity atom nearby, through a higher-order process involving the localized photons of both excited atoms. The localized photon of one of the excited atoms can under go virtual hop to the other excited atom, through RDDI, as discussed earlier. Such a photon-photon interaction gives rise to second-harmonic generation when a pair of excited atoms experience a close encounter and the propagation of the resulting high-energy photon out of the band gap. The lifetime for the decay of two neighboring excited atoms by such a spontaneous second-harmonic generation decreases inversely with the eighth power of the interatomic separation [8], and is estimated to

be on the order of milliseconds, when the distance between the atoms is 5 Å. This is still a very long lifetime for most practical purposes.

For an impurity atom embedded in a solid dielectric host, the vibrational modes of the host can provide an alternative relaxation mechanism for the photon-atom bound state by altering the electronic spectrum of the impurity [8]. We next give a simple semiquantitative discussion of phonon relaxation for the V system depicted Fig. 1(a). In a semiclassical picture, phonon interactions cause the energy levels of an atom to experience small, random, time-varying, Stark shifts. In our simplified picture, we assume that this phenomenon can be modeled by adding random shifts $\delta\omega_{j1}(t)$ to the energy differences ω_{j1}, $j=(2,3)$. The random functions $\delta\omega_{j1}(t)$ are as often positive as negative, and hence the ensemble averages $[\langle \delta\omega_{j1}(t)\rangle]$ are zero. Thus we can simulate phonon interaction by Gaussian random variables $\delta\omega_{ij}$ of zero mean and variance γ whose value depends on the strength of these interactions. Furthermore we assume that the phonon reservoir is Markovian [48] so that the averages of the products $\langle \delta\omega_{j1}(t)\,\delta\omega_{j1}(t')\rangle$ are zero unless $t\approx t'$. Assuming that variations in $\delta\omega_{j1}(t)$ are very rapid compared to other changes in the system, which occur on the time scale $1/\gamma_{j1}$, we take

$$\langle \delta\omega_{j1}(t)\,\delta\omega_{j1}(t')\rangle = \gamma_{j1d}\delta(t-t') \quad (j=2,3), \qquad (67)$$

where γ_{j1d} are the dephasing rates. Thus when phonon interactions are taken into account, Eqs. (63a) and (63b) have to be rewritten with δ_{j1} replaced by $\delta_{j1}+\delta\omega_{j1}(t)$ and ω_{32} by $\omega_{32}+\delta\omega_{31}(t)-\delta\omega_{21}(t)$, where δ_{j1}, and ω_{32} are the corresponding quantities in the absence of random stark shifts. For example if δ_{31} is set to zero, it means that, in the absence of stark shifts, the transition frequency ω_{31} coincides with the photonic band edge ω_a, and therefore the shifts $\delta\omega_{31}(t)$ slightly tune level $|3\rangle$ in and out of the band gap in a random fashion.

Figure 10 depicts the excited-state population $n_3(t)$ on level $|3\rangle$ as a function of the scaled time βt for $\delta=0$ and for different values of Ω, when $\delta\omega_{31}(t)$ and $\delta\omega_{21}(t)$ are taken as Gaussian random variables of zero mean and 0.5β variance. These and other numerical simulations show that, even when the dephasing rate γ_{31d} is comparable to β, the phase sensitive memory effects which we obtained without including dephasing effects, can be recaptured provided that the external Rabi frequency Ω is large compared to the dephasing rate. In other words, dephasing effects simply determine the minimum required intensity of the external laser field for achieving coherent control of radiative dynamics. The effect of the random shifts of the atomic levels $|2\rangle$ and $|3\rangle$ on the coherence $n_c(t)$ between the levels is shown in Fig. 11. We see that, just in the case of populations, these effects can be offset by intense driving fields.

VII. DISCUSSION AND CONCLUSIONS

In this paper we have investigated the coherent control of spontaneous emission from a three-level atom in a photonic band-gap structure with one resonance frequency near the edge of a photonic band gap. We have shown that spontaneous emission from the three-level atom can be totally suppressed or strongly enhanced depending on the relative phase between the control laser driving the two upper transitions and the pump laser used to create an excited state of the atom in the form of a coherent superposition of the two upper

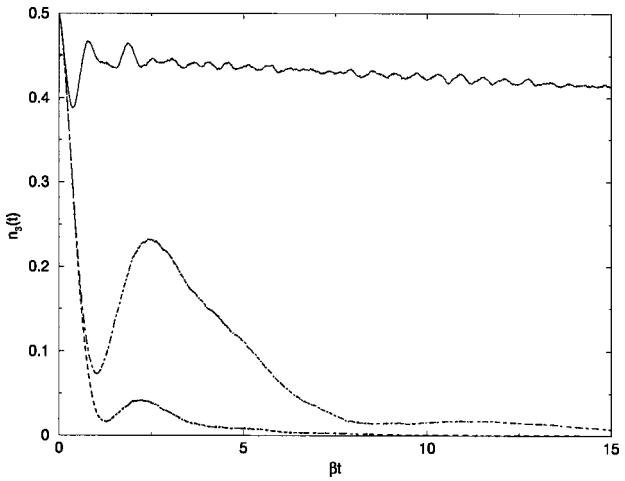

FIG. 10. V-system excited-state population $n_3(t)$ on level $|3\rangle$ near the isotropic photonic band edge as a function of the scaled time βt for $\theta=\pi/4$ and for the relative phase $\phi=-\pi/2$ in the presence of dipolar dephasing Gaussian random stark shifts $\delta\omega_{31}(t)$ and $\delta\omega_{21}(t)$ (each of zero mean and 0.5β variance) of the transition frequencies ω_{31} and ω_{21}. The different choices of the control laser amplitude are dashed curve ($\Omega=0$), dot-dashed curve ($\Omega=0.5\beta$), and solid curve ($\Omega=5\beta$). In the absence of the random Stark shifts, the band edge is assumed to be midway between the two upper levels with detuning $\delta_{31}=-\delta_{21}=0.5\beta$. Compare this figure with the corresponding figure [Fig. (9)] in the absence of phonon mediated dephasing.

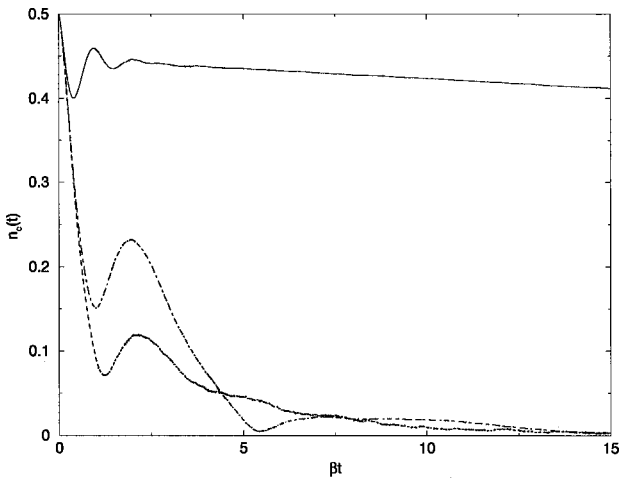

FIG. 11. V-system coherence $n_c(t)=|b_3(t)b_2^*(t)|$ between levels $|3\rangle$ and $|2\rangle$ near the isotropic photonic band edge as a function of the scaled time βt for $\theta=\pi/4$ and $\phi=-\pi/2$ in the presence of dipolar dephasing Gaussian random Stark shifts $\delta\omega_{31}(t)$ and $\delta\omega_{21}(t)$ (each of zero mean and 0.5β variance) of the transition frequencies ω_{31} and ω_{21}. The different choices of the control laser amplitude are dashed curve ($\Omega=0$), dot-dashed curve ($\Omega=0.5\beta$), and solid curve ($\Omega=5\beta$). In the absence of the random Stark shifts, the band edge is assumed to be midway between the two upper levels with detuning $\delta_{31}=-\delta_{21}=0.5\beta$. Compare this figure with the corresponding figure [Fig. (7)] in the absence of phonon-mediated dephasing.

levels. The steady-state atomic population on the upper levels of the three-level atom depends sensitively on the initial coherence as well as on the phase and intensity of the control laser field. This provides the basis for a quantum optical memory device on the atomic scale. For instance the two upper levels of the three-level system can be used as qubits to encode information for quantum computation. This model system may be realized by optically trapping cold atoms in the void fraction of a three-dimensional photonic band-gap material.

In determining the effects of the PBG on the emission dynamics of our model system, we employed the effective mass dispersion relation (31). Strictly speaking, such a dispersion relation is valid only near the edge of the gap. Therefore, the quantitative results derived from it cannot, in principle, be extrapolated to the whole gap. However, one expects that the effective-mass approximation gives qualitatively correct physics [8] and that a full dispersion relation may only introduce quantitative corrections. Even so, investigation of our model system using a full anisotropic dispersion relation of a realistic band structure [7,59] is a worthy undertaking. This would involve a realistic evaluation of the Green's-function [see, for instance, Eq. (A5)] using the full dispersion relation $\omega_{\mathbf{k}}$ appropriate to a real photonic crystal. The resulting equations of motion for radiative dynamics would then need to be solved numerically.

In our model system we assumed that single-photon spontaneous emission (on the transition $|2\rangle \rightarrow |1\rangle$ for the V configuration or on the transition $|3\rangle \rightarrow |2\rangle$ for the Λ configuration) is either forbidden (leading approximation) or leads to a photon-atom bound state in the presence of a complete photonic band gap. However, many of the effects we have described may be observable even in the absence of an ideal PBG. A complete 3D gap requires rather stringent material parameters. In many photonic crystals which do not have a complete gap, what one obtains more easily is a pseudogap, where the density of states is significantly reduced from that of free space but is not absolutely zero. In such a pseudogap, single-photon spontaneous decay will not be strictly forbidden but the decay rate will be significantly smaller than that in free space. If the depression in the local density of states [7] in the vicinity of the impurity atom is large enough as to make the spontaneous emission lifetime of an excited state inside the pseudogap longer than all other relevant time scales in the system, such a pseudogap, with the impurity atom suitably located, may lead to memory and coherent control effects that are qualitatively similar to those predicted in this paper.

Finally there is the question of how to place the active elements (the three-level atoms in our case) inside the photonic crystal. From a materials standpoint, it is possible to dope an existing PBG material using ion beam implantation methods. For example, it was recently shown that [60] erbium atoms implanted into bulk silicon exhibit sharp free-atom-like spectra. Intense photoluminescence at 1.54 μm is observed in the system at low temperatures. The radiative transition of this system arises from the atomic $4f$ shell which is effectively screened by outer shells from the crystal fields of the silicon background. It would be of considerable interest to study the radiative properties of erbium atoms implanted into a 3D silicon PBG material in which a photonic band gap is engineered to occur at 1.54 μm. For an inverse opal structure, composed of pure silicon, it is estimated [7] that such a PBG would occur for a fcc lattice of overlapping air spheres of diameter in the range 850–900 nm. In spite of the screening of the atomic transition by the outer shells, it is likely that thermal phonons in the silicon host would cause significant dephasing of the quantum degrees of freedom within the erbium $4f$ shell. Consequently such a system must be cooled to liquid-helium temperatures.

As discussed earlier, an alternative to ion implantation is that the active elements be incorporated inside a photonic crystal by pumping a dilute atomic vapor into the void region of the crystal. If such atoms are optically trapped in the void regions, they are not in mechanical contact with the vibrational degrees of freedom of the dielectric host and therefore do not experience phonon dephasing effects as in the case of erbium-doped silicon. Doppler broadening due to the random motion of the gas molecules may be partially alleviated by laser-cooling techniques [61].

A third approach to realize our model system is by means of an ''artificial atom'' or quantum dot structure embedded in the solid fraction of the PBG material. Semiconductor quantum dots (QD's) are nanoscale quantum structures that allow electronic properties to be tailored through quantum confinement. They exhibit distinctive features similar to atoms such as atomiclike excitation spectra with discrete and extremely sharp spectral lines [62]. With their well-defined localized states, QD's offer the possibility of coherent manipulation of a single localized quantum system in a way similar to that achieved in atoms but with the technological advantages of a solid-state system. The coherent optical control of an exciton wave function in a QD and, in particular, the manipulation of the relative phases of the eigenstates in a quantum superposition of states, was demonstrated in Ref. [63]. QD structures with stronger confinement are expected to have reduced coupling to phonons [64] and reduced spontaneous radiative emission [65], and may well have much longer intrinsic coherence times. These properties of QD's, which are necessary for the implementation of various schemes for quantum computation and coherent information processing, will be further enhanced by incorporating the QD's within a PBG material.

ACKNOWLEDGMENTS

This work was supported in part by the New Energy and Industrial Technology Development Organization (NEDO) of Japan, the Natural Sciences and Engineering Research Council of Canada, and Photonics Research Ontario. M.W. wishes to acknowledge Dr. Tran Quang for his very informative discussions, comments, and suggestions.

APPENDIX A: NON-MARKOVIAN MEMORY KERNELS

In this appendix we will derive the various expressions for the Green's functions used in the text. We start from Eq. (52),

$$G_{lm}(t-t') = \sum_{\mathbf{k}\lambda} g^{l1}_{\mathbf{k}\lambda} g^{m1}_{\mathbf{k}\lambda} e^{-i\mu^{m1}_{\mathbf{k}}(t-t')} \quad (l,m=2,3), \tag{A1}$$

where $\mu_{\mathbf{k}}^{m1}=\omega_{\mathbf{k}}-\omega_{m1}$. When $l=m$, Eq. (A1) reduces to Eq. (18). Substituting for $g_{\mathbf{k}\lambda}^{l1}$ and $g_{\mathbf{k}\lambda}^{m1}$ from Eq. (48), we obtain

$$G_{lm}(t-t')=\frac{\zeta}{V}\sum_{\mathbf{k}\lambda}(\hat{\mathbf{e}}_{\mathbf{k}\lambda}\cdot\hat{\mathbf{d}}_{l1})(\hat{\mathbf{e}}_{\mathbf{k}\lambda}\cdot\hat{\mathbf{d}}_{m1})\frac{1}{\omega_{\mathbf{k}}}e^{-i\mu_{\mathbf{k}}^{m1}(t-t')}, \tag{A2}$$

where

$$\zeta=\sqrt{\left(\frac{\omega_{l1}^2 d_{l1}^2}{2\hbar\epsilon_o}\right)\left(\frac{\omega_{m1}^2 d_{m1}^2}{2\hbar\epsilon_o}\right)}. \tag{A3}$$

Assuming that the modes of the field are closely spaced in frequency, we make the continuum approximation for the field modes and replace the summation over $\mathbf{k}$ by an integral,

$$\sum_{\mathbf{k}}\rightarrow\frac{V}{(2\pi)^3}\int d^3\mathbf{k}, \tag{A4}$$

where $d^3\mathbf{k}\equiv k^2 dk d\Omega$, $d\Omega$ being the space angle element. Thus

$$G_{lm}(t-t')=\frac{\zeta}{(2\pi)^3}\frac{8\pi}{3}\int\left[\frac{3}{8\pi}\sum_{\lambda}(\hat{\mathbf{e}}_{\mathbf{k}\lambda}\cdot\hat{\mathbf{d}}_{l1})\times(\hat{\mathbf{e}}_{\mathbf{k}\lambda}\cdot\hat{\mathbf{d}}_{m1})\right]\frac{1}{\omega_{\mathbf{k}}}e^{-i(\omega_{\mathbf{k}}-\omega_{m1})(t-t')}d^3\mathbf{k}. \tag{A5}$$

This is a general result valid for any dispersion relation $\omega_{\mathbf{k}}$. When the dispersion relation is isotropic (i.e., when $\omega_{\mathbf{k}}$ depends only on the magnitude k of $\mathbf{k}$), Eq. (A5) reduces to

$$G_{lm}(t-t')=\frac{\zeta}{(2\pi)^3}\frac{8\pi}{3}\eta_{lm}\int_0^{\Lambda}\frac{1}{\omega_k}e^{-i(\omega_k-\omega_{m1})(t-t')}k^2 dk, \tag{A6}$$

where

$$\eta_{lm}=\frac{3}{8\pi}\int\sum_{\lambda}(\hat{\mathbf{e}}_{\mathbf{k}\lambda}\cdot\hat{\mathbf{d}}_{l1})(\hat{\mathbf{e}}_{\mathbf{k}\lambda}\cdot\hat{\mathbf{d}}_{m1})d\Omega, \tag{A7}$$

and $\Lambda=mc/\hbar$ is the Compton wave number of the electron. We have introduced the cutoff Λ in the photon wave vector [66] as the contributions of extremely high-energy photons cannot be important. The the nonrelativistic approximation for the electron is not be valid for photons of energy $\hbar\omega\sim mc^2$. Consider a coordinate system defined by the unit vectors $\{\hat{\mathbf{e}}_{\mathbf{k}1},\hat{\mathbf{e}}_{\mathbf{k}2},\hat{\mathbf{k}}\}$. Defining $\{\alpha_{j1},\beta_{j1},\theta_{j1}\}$ as the direction angles of the dipole moment unit vector $\hat{\mathbf{d}}_{j1}$ $(j=l,m)$,

$$\eta_{lm}=\frac{3}{8\pi}\int(\cos\alpha_{l1}\cos\alpha_{m1}+\cos\beta_{l1}\cos\beta_{m1})d\Omega. \tag{A8}$$

If the dipoles $\hat{\mathbf{d}}_{l1}$ and $\hat{\mathbf{d}}_{m1}$ are parallel or antiparallel (so that $\alpha_{l1}=\pm\alpha_{m1}=\alpha$, $\beta_{l1}=\pm\beta_{m1}=\beta$, and $\theta_{l1}=\pm\theta_{m1}=\theta$), the law of direction cosines gives

$$\cos\alpha_{l1}\cos\alpha_{m1}+\cos\beta_{l1}\cos\beta_{m1}=\cos^2\alpha+\cos^2\beta=1-\cos^2\theta. \tag{A9}$$

Using this in Eq. (A8) we obtain $\eta_{lm}=1$. It follows that

$$\eta_{lm}=\delta_{lm}+\eta(1-\delta_{lm}), \tag{A10}$$

where δ_{lm} is the Kröonecker delta function, and

$$\eta=\frac{3}{8\pi}\int(\cos\alpha_{31}\cos\alpha_{21}+\cos\beta_{31}\cos\beta_{21})d\Omega. \tag{A11}$$

Thus $\eta=1$, when $\hat{\mathbf{d}}_{l1}=\pm\hat{\mathbf{d}}_{m1}$.

For vacuum we use the isotropic dispersion relation $\omega_k=ck$. The emitted radiation is centered about the atomic transition frequency $\omega_k=\omega_{m1}$; the quantity ω_k varies very little around $\omega_k=\omega_{m1}$. We can, therefore, replace k^2/ω_k in Eq. (A6) by ω_{m1}/c^2 and extend the limits of integration to $\pm\infty$ to obtain

$$G_{lm}(t-t')=\frac{\zeta\omega_{m1}}{(2\pi c)^3}\frac{8\pi}{3}\eta_{lm}\int_{-\infty}^{\infty}e^{-i(\omega_k-\omega_{m1})(t-t')}d\omega_k. \tag{A12}$$

In other words,

$$G_{lm}(t-t')=\eta_{lm}\sqrt{\gamma_{l1}\gamma_{m1}(\omega_{m1}/\omega_{l1})}\,\delta(t-t'), \tag{A13}$$

where

$$\gamma_{j1}=\frac{1}{4\pi\epsilon_o}\frac{4\omega_{j1}^3 d_{j1}^2}{3\hbar c^3}\quad(j=3,2) \tag{A14}$$

is the vacuum spontaneous emission rate for the transition $|j\rangle\rightarrow|1\rangle$. Assuming that the upper levels $|3\rangle$ and $|2\rangle$ are close together so that $\omega_{m1}/\omega_{l1}\approx 1$, we finally obtain

$$G_{lm}(t-t')=\eta_{lm}\sqrt{\gamma_{l1}\gamma_{m1}}\,\delta(t-t'). \tag{A15}$$

For a PBG material described by the isotropic effective-mass dispersion relation (30), Eq. (A5) takes the form

$$G_{lm}(t-t')=\frac{\zeta}{(2\pi)^3}\frac{8\pi}{3}\eta_{lm}e^{i\delta_{m1}(t-t')}\times\int_{k_0}^{\Lambda}\frac{k^2 e^{-iA(k-k_0)^2(t-t')}}{\omega_c+A(k-k_0)^2}dk, \tag{A16}$$

where $\delta_{m1}=\omega_{m1}-\omega_a$ is the detuning of the atomic transition frequency ω_{m1} from the band-edge frequency ω_a. The integral in Eq. (A16) can be approximated by replacing k by k_0 outside of the exponential and extending the wave-vector integration to infinity, which then reduces to a complex Fresnel integral given by [67]

$$\int_0^{\infty}e^{-iAu^2(t-t')}du=\frac{e^{-i\pi/4}}{2\sqrt{A}}\sqrt{\frac{\pi}{t-t'}}. \tag{A17}$$

Using Eq. (A3) and the fact that $A\approx\omega_c/k_0^2$, we obtain

$$G_{lm}(t-t')=\eta_{lm}\sqrt{\beta_{l1}^{3/2}\beta_{m1}^{3/2}}\frac{e^{i[\delta_{m1}(t-t')-\pi/4]}}{\sqrt{\pi(t-t')}}, \quad \text{(A18)}$$

where

$$\beta_{j1}^{3/2}=\frac{1}{4\pi\epsilon_o}\frac{\omega_{j1}^2\omega_c^{3/2}d_{j1}^2}{3\hbar c^3}. \quad \text{(A19)}$$

This expression may be further simplified by assuming that the upper levels $|3\rangle$ and $|2\rangle$ are close together so that $\omega_{31}\approx\omega_{21}\approx\omega_a$. We then have

$$\sqrt{\beta_{21}^{3/2}\beta_{31}^{3/2}}\approx\beta^{3/2}\equiv\frac{1}{4\pi\epsilon_o}\frac{\omega_{31}^{7/2}d_{31}^2}{3\hbar c^3}. \quad \text{(A20)}$$

As shown previously [10], for a two-level atom placed inside a photonic crystal of band-edge frequency nearly resonant with the atomic transition frequency, the upper level splits into a doublet because of the strong interaction between the atom and its own localized radiation. β gives the magnitude of this frequency splitting for the isotropic dispersion relation (30). The dipole moment of a hydrogenic (that is, one electron) atom can be approximated by $d_{31}\sim ea_0$, where e is the magnitude of the electronic charge and $a_0\sim 0.5$ Å is the Bohr radius. Moreover for optical transition frequencies $\omega_{31}\sim 10^{15}$ Hz. Using these in Eq. (A19) we obtain $\beta\sim 10^{-7}\omega_a$. Thus when the band edge ω_a is in the optical regime, β will be comparable to the ordinary Lamb shift of the $2S_{1/2}$ level of hydrogen [8].

For a PBG material described by the anisotropic effective-mass dispersion relation (31), the general expression (A2) takes the form

$$G_{lm}(t-t')=\frac{\zeta}{(2\pi)^3}\frac{8\pi}{3}e^{i\delta_{m1}(t-t')}\int\left[\frac{3}{8\pi}\sum_{\lambda}(\hat{\mathbf{e}}_{\mathbf{k}\lambda}\cdot\hat{\mathbf{d}}_{l1})\times(\hat{\mathbf{e}}_{\mathbf{k}\lambda}\cdot\hat{\mathbf{d}}_{m1})\right]\frac{e^{-iA(\mathbf{k}-\mathbf{k}_0)^2(t-t')}}{\omega_c+A(\mathbf{k}-\mathbf{k}_0)^2}d^3\mathbf{k}. \quad \text{(A21)}$$

Making the substitution $\mathbf{q}=\mathbf{k}-\mathbf{k}_0$, so that $d^3\mathbf{q}=q^2dqd\Omega$, performing the angular integration, and extending the wave-vector integration to infinity, we obtain

$$G_{lm}(t-t')=\frac{\zeta}{(2\pi)^3}\frac{8\pi}{3}\eta_{lm}e^{i\delta_{m1}(t-t')}\frac{1}{A}\times\int_0^\infty\frac{e^{-iAq^2(t-t')}}{\omega_c/A+q^2}q^2dq, \quad \text{(A22)}$$

where η_{lm} is given by Eq. (A8). For large $t-t'$, the integral in Eq. (A22) is dominated by the stationary phase point $q=0$. This yields (using $\int_0^\infty x^2e^{-ax^2}dx=\sqrt{\pi}a^{-3/2}/4$)

$$G_{lm}(t-t')=-\eta_{lm}\sqrt{\alpha_{l1}\alpha_{m1}}\frac{e^{i[\delta_{m1}(t-t')+\pi/4]}}{\sqrt{4\pi(t-t')^3}} \quad \omega_c(t-t')\gg 1, \quad \text{(A23)}$$

where

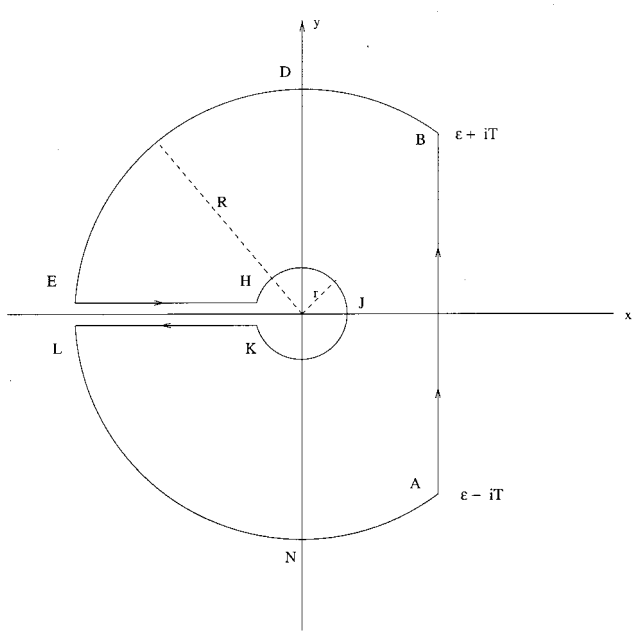

FIG. 12. The contour used in the complex inversion formula (B1).

$$\alpha_{j1}=\frac{1}{4\pi\epsilon_o}\frac{\omega_{j1}^2\omega_c^{1/2}d_{j1}^2}{3\hbar c^3}. \quad \text{(A24)}$$

Equation (A23) may be further simplified by assuming that the upper levels $|3\rangle$ and $|2\rangle$ are close together so that $\omega_{31}\approx\omega_{21}\approx\omega_a$. We then have

$$\sqrt{\alpha_{21}\alpha_{31}}\approx\alpha\equiv\frac{1}{4\pi\epsilon_o}\frac{\omega_{31}^{5/2}d_{31}^2}{3\hbar c^3}. \quad \text{(A25)}$$

The full expression of $G_{lm}(t-t')$, including its short-time behavior, is given elsewhere [49].

APPENDIX B: TIME DEPENDENCE OF THE ATOMIC AMPLITUDES AND THE STRONG-FIELD LIMIT

The amplitudes $b_{2,3}(t)$ are found from the inverse Laplace transform of the expressions for $\tilde{b}_{2,3}(s+i\delta)$ given by Eqs. (36a) and (36b) through the complex inversion formula

$$e^{-i\delta t}b_j(t)=\frac{1}{2\pi i}\int_{\epsilon-i\infty}^{\epsilon+i\infty}e^{st}\tilde{b}_j(s+i\delta)ds. \quad \text{(B1)}$$

Here the real number ϵ is chosen so that $s=\epsilon$ lies to the right of all the singularities (poles and branch points) of the functions $\tilde{b}_{2,3}(s+i\delta)$. It is apparent from Eq. (37) that $s=0$ is a branch point of both $\tilde{b}_{2,3}(s+i\delta)$. In order to evaluate Eq. (B1), we consider the contour C shown in Fig. 12, where the branch cut of the integrand is chosen to lie along the negative real axis. According to the residue theorem,

$$\frac{1}{2\pi i}\oint_C e^{st}\tilde{b}_j(s+i\delta)ds=R_{\text{sum}}, \quad \text{(B2)}$$

where $R_{\rm sum}$ is the sum of the residues of the integrand at the poles enclosed by the contour C. Omitting the integrand, we have

$$R_{\rm sum}=\frac{1}{2\pi i}\oint_C=\frac{1}{2\pi i}\times\left(\int_{AB}+\int_{BDE}+\int_{EH}+\int_{HJK}+\int_{KL}+\int_{LNA}\right). \tag{B3}$$

In the limit $r\to 0$ and $R\to\infty$ (so that $T\to\infty$), the second, fourth, and sixth integrals on the right-hand side of Eq. (B3) approach zero and, according to Eq. (B1), the first integral gives $e^{-i\delta t}b_3(t)$. Thus

$$e^{-i\delta t}b_j(t)=R_{\rm sum}-\lim_{R\to\infty,r\to 0}\frac{1}{2\pi i}\left(\int_{EH}+\int_{KL}\right). \tag{B4}$$

We first calculate $b_3(t)$. Along EH, $s=xe^{i\pi}=-x$. Using this in Eq. (36a), we obtain

$$\lim_{R\to\infty,r\to 0}\int_{EH}e^{st}\tilde{b}_3(s+i\delta)ds=\int_0^\infty\frac{[(-x+i\delta)\cos\theta-\Omega e^{i\phi}\sin\theta]e^{-xt}}{(-x+i\delta)^2-\alpha e^{-i\pi/4}(-x+i\delta)\sqrt{x}+\Omega^2}dx. \tag{B5}$$

Similarly, along KL, $s=xe^{-i\pi}=-x$. Using this in Eq. (36a), we obtain

$$\lim_{R\to\infty,r\to 0}\int_{KL}e^{st}\tilde{b}_3(s+i\delta)ds=-\int_0^\infty\frac{[(-x+i\delta)\cos\theta-\Omega e^{i\phi}\sin\theta]e^{-xt}}{(-x+i\delta)^2+\alpha e^{-i\pi/4}(-x+i\delta)\sqrt{x}+\Omega^2}dx. \tag{B6}$$

Using Eqs. (B5) and (B6) in Eq. (B4), we then obtain

$$e^{-i\delta t}b_3(t)=R_{\rm sum}+\frac{\alpha e^{i\pi/4}}{\pi}\int_0^\infty\frac{g_3(x)e^{-(x-i\delta)t}}{Z(x)}dx, \tag{B7}$$

where

$$g_3(x)=[(-x+i\delta)\cos\theta-\Omega e^{i\phi}\sin\theta](-x+i\delta)\sqrt{x}, \tag{B8a}$$

$$Z(x)=[(-x+i\delta)^2+\Omega^2]^2+i\alpha^2(-x+i\delta)^2x. \tag{B8b}$$

Next we evaluate the total residue $R_{\rm sum}$. From Eqs. (36a) and (37), we have

$$e^{st}\tilde{b}_3(s+i\delta)=[(s+i\delta)\cos\theta-\Omega e^{i\phi}\sin\theta]e^{st}\times\prod_{j=1}^4\frac{\sqrt{s}+e^{i\pi/4}u_j}{s-iu_j^2}. \tag{B9}$$

Clearly, the function $e^{st}\tilde{b}_3(s+i\delta)$ has simple poles at $s=iu_j^2$, $(j=1,\ldots,4)$. The residue R_k at $s=iu_k^2$ is then

$$R_k\equiv\lim_{s\to iu_k^2}(s-iu_k^2)e^{st}\tilde{b}_3(s+i\delta)=[(u_k^2+\delta)\cos\theta+i\Omega e^{i\phi}\sin\theta]e^{iu_k^2t}\frac{(\sqrt{u_k^2+u_1})\cdots(\sqrt{u_k^2+u_4})}{(u_k^2-u_l^2)(u_k^2-u_m^2)(u_k^2-u_n^2)}\quad(k\neq l\neq m\neq n). \tag{B10}$$

Numerical examinations show that the roots $u_{1,3}$ are real (u_1 is positive but u_3 is negative). The roots $u_{2,4}$ are complex conjugates of each other with a negative real part (u_2 and u_4 lie in the third and second quadrants, respectively). Thus the negative root u_3 lies outside the contour C, so that the residue at u_3 is $R_3=0$. For the complex root u_4 (which has a positive imaginary part), the factor $e^{iu_4^2t}$ increases exponentially in time and therefore is unphysical. Thus for this root we choose the negative branch of the square root function and set $\sqrt{u_4^2}+u_4=0$ so that the residue at u_4 is $R_4=0$. On the other hand, for the positive root u_1 and the complex root u_2 we choose the positive branch of the square root function and set $\sqrt{u_j^2}=u_j$, $(j=1,2)$. The residues at u_1 and u_2 are

$$R_j=P_jQ_{3j}e^{iu_j^2t}\quad(j=1,2), \tag{B11}$$

where

$$P_j=\frac{2u_j}{(u_j-u_l)(u_j-u_m)(u_j-u_n)}\quad(l,m,n=1,\ldots,4,j\neq l\neq m\neq n), \tag{B12a}$$

$$Q_{3j}=(u_j^2+\delta)\cos\theta+i\Omega e^{i\phi}\sin\theta. \tag{B12b}$$

The sum of the residues of the function $e^{st}\tilde{b}_3(s+i\delta)$ is then

$$R_{\rm sum}=\sum_{k=1}^4R_k=\sum_{j=1}^2P_jQ_{3j}e^{iu_j^2t}. \tag{B13}$$

Using this in Eq. (B7), we finally arrive at the desired result (41a). Following exactly the same procedure, we also find that

$$b_2(t)=\sum_{j=1}^2P_jQ_{2j}e^{i(u_j^2+\delta)t}+\frac{\alpha\Omega e^{i(\phi_c-\pi/4)}}{\pi}\int_0^\infty\frac{g_2(x)e^{-(x-i\delta)t}}{Z(x)}dx, \tag{B14}$$

where P_j and $Z(x)$ are the same as those for $b_3(t)$ and

$$Q_{2j}=(u_j^2+\alpha u_j+\delta)e^{i\phi_p}\sin\theta-i\Omega e^{i\phi_c}\cos\theta, \tag{B15a}$$

$$g_2(x)=[(-x+i\delta)\cos\theta-\Omega e^{i\phi}\sin\theta]\sqrt{x}. \tag{B15b}$$

For a very strong control laser field (when $\Omega\gg\alpha^2,\delta$) the roots given by Eqs. (39a) and (39b) satisfy $u_1\sim\sqrt{\Omega}$, $u_2\sim-\sqrt{\Omega}$ and $u_2=u_4^*\sim-\sigma_2-i\sqrt{\Omega}$ so that $P_1\sim 1/2\Omega$,

$$Q_{31}\sim\Omega[\cos\theta+ie^{i\phi}\sin\theta], \tag{B16a}$$

$$Q_{21} \sim -i\Omega e^{i\phi_c}[\cos\theta + ie^{i\phi}\sin\theta]. \tag{B16b}$$

Using these in Eqs. (43) and (45), we obtain

$$n_{3s} \approx n_{2s} \approx \frac{1}{4}(1-\sin 2\theta \sin\phi), \tag{B17a}$$

$$b_3(t)b_2^*(t) \approx \frac{ie^{-i\phi_c}}{4}(1-\sin 2\theta\sin\phi) \tag{B17b}$$

for the steady-state values of populations and coherences in the limit of a strong driving field.

APPENDIX C: QUANTUM BEAT CASE

When $\Omega=0$, Eqs. (63a) and (63b) can be solved by means of Laplace transformations to give closed analytic expressions for the amplitudes $h_{2,3}(t)$. These expressions take particularly simple forms when the band edge ω_a is midway between the two upper of levels of the V system (so that $\delta_{31}=-\delta_{21}=\delta \geqslant 0$) and when the atomic dipoles associated with the transitions $|3\rangle \rightarrow |1\rangle$ and $|2\rangle \rightarrow |1\rangle$ are parallel or antiparallel (so that $\eta=1$). In this special case Eqs. (63a) and (63b) reduce to

$$\dot{h}_2(t) = i\delta h_2(t) - \int_0^t G(t-t')[h_2(t')+h_3(t')]dt', \tag{C1a}$$

$$\dot{h}_3(t) = -i\delta h_3(t) - \int_0^t G(t-t')[h_2(t')+h_3(t')]dt'. \tag{C1b}$$

Upon taking the Laplace transforms of these equations, we find that

$$\tilde{h}_2(s) = \frac{(s+i\delta)b_2(0) - \rho e^{i\pi/4}\sqrt{s}}{D(s)}, \tag{C2a}$$

$$\tilde{h}_3(s) = \frac{(s-i\delta)b_3(0) + \rho e^{i\pi/4}\sqrt{s}}{D(s)}, \tag{C2b}$$

where

$$\rho = \alpha[b_3(0)-b_2(0)], \tag{C3a}$$

$$D(s) = s^2 + 2\alpha e^{i\pi/4}s\sqrt{s} - \delta^2 = \prod_{j=1}^{4}(\sqrt{s} - e^{i\pi/4}v_j), \tag{C3b}$$

and α is defined in Eq. (33). Here $v_j (j=1,\ldots,4)$ are the roots of the quartic $x^4 + 2\alpha x^3 - \delta^2 = 0$ and are given by [50]

$$v_{1,3} = -\sigma_1/2 \pm \sqrt{(\sigma_1/2)^2 - \xi_2}, \tag{C4a}$$

$$v_2 = v_4^* = -\sigma_2/2 - i\sqrt{\xi_1 - (\sigma_2/2)^2}, \tag{C4b}$$

$$\sigma_{1,2} = \alpha \pm \sqrt{\alpha^2 + u}, \tag{C4c}$$

$$\xi_{1,2} = u/2 \pm \sqrt{(u/2)^2 + \delta^2}, \tag{C4d}$$

$$u = -(2\alpha^2\delta^2)^{1/3}\ [(A+1)^{1/3} - (A-1)^{1/3}], \tag{C4e}$$

$$A = [1 + (4/27)(2\delta/a^2)^6]^{1/2}. \tag{C4f}$$

Equation (C4e) shows that the quantity u is always negative. Thus ξ_1 and $\sigma_{1,2}$ are positive whereas ξ_2 is negative. It follows that the roots

$$v_{1,3} = -|\sigma_1|/2 \pm \sqrt{(\sigma_1/2)^2 + |\xi_2|} \tag{C5}$$

are both real. Moreover, numerical analysis shows that $\xi_1 - (\sigma_1/2)^2 \geqslant 0$ for all δ. The equality sign holds for $\delta=0$ (i.e., when the upper levels $|3\rangle$ and $|2\rangle$ are degenerate). Thus

$$v_2 = v_4^* = -\sigma_2/2 - i\sqrt{|\xi_1 - (\sigma_2/2)^2|}, \tag{C6}$$

so that the roots v_2 and v_4 are complex conjugates of each other. Equations (C2a) and (C2b) can now be inverted (following the procedure described in Appendix B), to give

$$b_3(t) = \sum_{j=1}^{2} E_j F_{3j} e^{i(v_j^2+\delta)t} + \frac{e^{i\pi/4}}{\pi}\int_0^\infty \frac{f_3(x)e^{-(x-i\delta)t}dx}{W(x)}, \tag{C7a}$$

$$b_2(t) = \sum_{j=1}^{2} E_j F_{2j} e^{i(v_j^2-\delta)t} + \frac{e^{i\pi/4}}{\pi}\int_0^\infty \frac{f_2(x)e^{-(x+i\delta)t}dx}{W(x)}, \tag{C7b}$$

where

$$E_j = \frac{2v_j}{(v_j-v_l)(v_j-v_m)(v_j-v_n)}$$

$$(l,m,n=1,\ldots,4, j\neq l\neq m\neq n), \tag{C8a}$$

$$F_{3j} = (v_j^2-\delta)b_3(0) + v_j\rho = (v_j^2+\alpha v_j-\delta)b_3(0) - \alpha v_j b_2(0), \tag{C8b}$$

$$F_{2j} = (v_j^2+\delta)b_3(0) - v_j\rho = (v_j^2+\alpha v_j+\delta)b_2(0) - \alpha v_j b_3(0), \tag{C8c}$$

$$f_3(x) = [-\rho(x^2+\delta^2) + 2\alpha b_3(0)(x+i\delta)x]\sqrt{x}, \tag{C8d}$$

$$f_2(x) = [\rho(x^2+\delta^2) + 2\alpha b_2(0)(x-i\delta)x]\sqrt{x}, \tag{C8e}$$

$$W(x) = (x^2+\delta^2)^2 + i4\alpha^2x^3. \tag{C8f}$$

APPENDIX D: TWO-LEVEL ATOM

Consider the special case of our model system when $\Omega=0$, i.e., when the upper levels $|3\rangle$ and $|2\rangle$ are not driven by a control laser field and single-photon spontaneous emission for the transition $|2\rangle \rightarrow |1\rangle$ is assumed to be forbidden. This means that the population of level $|2\rangle$ cannot decay directly to level $|1\rangle$. Its only decay mechanism is indirectly through level $|3\rangle$ via the coupling Ω. If $\Omega=0$, level $|2\rangle$ will be completely decoupled from the rest of the system, and our model system of Fig. 1 is effectively a two-level system consisting of levels $|3\rangle$ and $|1\rangle$. In this case Eqs. (19a) and

(19b) reduce (assuming that the atom is initially on the upper level $|3\rangle$ so that $\theta=0$) to $\tilde{b}_2(s)=0$ and

$$\tilde{b}_3(s)=\frac{1}{s+\tilde{G}(s)}. \tag{D1}$$

Using Eq. (35), this can be written as

$$\tilde{b}_3(s+i\delta)=1/D(s), \tag{D2}$$

where

$$D(s)=s+\alpha e^{i\pi/4}\sqrt{s}+i\delta=\prod_{j=1}^{2}(\sqrt{s}-e^{i\pi/4}v_j). \tag{D3}$$

Here v_j $(j=1,2)$ are the roots of the quadratic equation $x^2+\alpha x+\delta=0$, and are given by

$$v_{1,2}=-\frac{\alpha}{2}\pm\sqrt{\left(\frac{\alpha}{2}\right)^2-\delta}. \tag{D4}$$

The amplitude $b_3(t)$ is found from the inverse Laplace transform of $\tilde{b}_3(s+i\delta)$ through the inversion integral of Eq. (B1). Following the method of Appendix B and using the contour of Fig. 12 yields the results listed below:

(a) If $\delta<0$ (upper level $|3\rangle$ is inside the gap), roots (D4) are given by

$$r_{1,2}=-\frac{\alpha}{2}\pm\sqrt{\left(\frac{\alpha}{2}\right)^2+|\delta|}. \tag{D5}$$

Thus r_1 is positive, whereas r_2 is negative and lies outside the contour of integration. In this case we obtain

$$b_3(t)=c_1e^{i(r_1^2+\delta)t}+I(\delta,t) \quad \delta<0, \tag{D6}$$

where $c_1=2r_1/(r_1-r_2)$, and the branch cut contribution

$$I(\delta,t)=\frac{\alpha e^{i\pi/4}}{\pi}\int_0^\infty\frac{\sqrt{x}e^{(-x+i\delta)t}}{(-x+i\delta)^2+i\alpha^2x}dx \tag{D7}$$

tends to zero as $t\to\infty$.

(b) If $0\leqslant\delta\leqslant(\alpha/2)^2$, both roots $v_{1,2}$ are negative and lie outside the contour of integration. In this case we obtain

$$b_3(t)=I(\delta,t), \quad 0\leqslant\delta\leqslant(\alpha/2)^2 \tag{D8}$$

where $I(\delta,t)$ is given by Eq. (D7).

(c) If $\delta>(\alpha/2)^2$, roots (D4) are complex conjugates of each other given by

$$w_1=w_2^*=-\frac{\alpha}{2}-i\sqrt{|\delta|-\left(\frac{\alpha}{2}\right)^2}. \tag{D9}$$

In this case the residue corresponding to w_2 is zero and we obtain

$$b_3(t)=d_1e^{i(w_1^2+\delta)t}+I(\delta,t), \quad \delta>(\alpha/2)^2 \tag{D10}$$

where $d_1=2w_1\cos\theta/(w_1-w_2)$.

Since the root r_1 is positive while the root w_1 is complex with a negative real part, the first term on the right-hand side of Eq. (D6) is a nondecaying oscillatory term while that of Eq. (D10) decays in time and tends to zero as $t\to\infty$. The term $I(\delta,t)$ also decays in time and tends to zero as $t\to\infty$. The steady-state population on the upper level $|3\rangle$ is then given by

$$n_{3s}\equiv\lim_{t\to\infty}|b_3(t)|^2=\begin{cases}4r_1^2/(r_1-r_2)^2 & \text{if } \delta<0\\ 0 & \text{if } \delta\geqslant 0.\end{cases} \tag{D11}$$

Thus for the two-level system (consisting of the ground level $|1\rangle$ and the excited level $|3\rangle$) placed inside a PBG structure described by the effective mass anisotropic dispersion relation [Eq. (31)], fractionalized steady-state inversion occurs only for $\delta<0$ (i.e., for $\omega_{31}<w_a$). On the other hand, for such a two-level system in the isotropic model [Eq. (30)], it was shown [10] that fractionalized inversion occurs even when ω_{31} is slightly greater than ω_a, that is, even when the excited state lies *outside* (but not far from) the band gap.

[1] E. M. Purcell, Phys. Rev. **69**, 681 (1946).
[2] E. A. Hinds, Adv. At., Mol., Opt. Phys. **28**, 237 (1991).
[3] M. Lewenstein, J. Zakrzewski, T. M. Mossberg, and J. Mostowski, J. Phys. B **21**, L9 (1988); M. Lewenstein, J. Zakrzewski, and T. M. Mossberg, Phys. Rev. A **38**, 1075 (1988).
[4] S. John, Phys. Rev. Lett. **53**, 2169 (1984).
[5] E. Yablonovitch, Phys. Rev. Lett. **58**, 2059 (1987).
[6] S. John, Phys. Rev. Lett. **58**, 2486 (1987).
[7] K. Busch and S. John, Phys. Rev. E **58**, 3896 (1998), and references therein.
[8] S. John and J. Wang, Phys. Rev. Lett. **64**, 2418 (1990); Phys. Rev. B **43**, 12 772 (1991); S. John, in *Confined Electrons and Photons*, edited by E. Burstein and C. Weisbuch (Plenum, New York, 1995).
[9] R. F. Nabiev, P. Yeh, and J. J. Sanchez-Mondragon, Phys. Rev. A **47**, 3380 (1993).
[10] S. John and Tran Quang, Phys. Rev. A **50**, 1764 (1994).
[11] S. John and Tran Quang, Phys. Rev. Lett. **74**, 3419 (1995).
[12] S. John and Tran Quang, Phys. Rev. A **52**, 4083 (1995).
[13] E. Yablonovitch, J. Opt. Soc. Am. B **10**, 283 (1993).
[14] E. T. Jaynes and F. W. Cummings, Proc. IEEE **51**, 89 (1963).
[15] J. D. Joannopoulos, R. D. Meade, and J. N. Winn, *Photonic Crystals* (Princeton University Press, Princeton, 1995).
[16] J. C. Knight, J. Broeng, T. A. Birks, and P. St. J. Russell, Science **282**, 1476 (1998), and references therein.
[17] E. Yablonovitch, T. J. Gmitter, and K. M. Leung, Phys. Rev. Lett. **67**, 2295 (1991). For a review of recent progress in the microfabrication of PBG materials, see *Photonic Band Gap Materials*, Vol. 315 of *NATO Advanced Study Institute, Series E: Photonic Band Gap Materials*, edited by C. M. Soukoulis (Kluwer, Dordrecht, 1996).
[18] U. Gruning, V. Lehmann, S. Ottow, and K. Busch, Appl. Phys. Lett. **68**, 747 (1996).
[19] E. N. Economou and M. M. Sigalas, Phys. Rev. B **48**, 13 434 (1993).

[20] N. Yamamoto, S. Noda, and A. Chutinan, Jpn. J. Appl. Phys. **37**, L1052 (1998).
[21] S. Lin *et al.*, Nature (London) **394**, 251 (1998).
[22] S. Mann and G. A. Ozin, Nature (London) **382**, 213 (1996).
[23] I. I. Tarhan and G. H. Watson, Phys. Rev. Lett. **76**, 315 (1996).
[24] R. D. Pradhan, J. A. Bloodgood, and G. H. Watson, Phys. Rev. B **55**, 9503 (1997).
[25] W. L. Vos, R. Sprik, A. van Blaaderen, A. Imhof, A. Lagendijk, and G. H. Weydam, Phys. Rev. B **53**, 16 231 (1996); W. L. Vos, M. Megens, C. M. van Kats, and P. Bosecke, J. Phys.: Condens. Matter **8**, 9503 (1996).
[26] Yu. A. Vlasov, V. N. Astratov, O. L. Karimov, A. A. Kaplyanskii, V. N. Bogomolov, and A. V. Prokofiev, Phys. Rev. B **55**, R13357 (1997).
[27] V. N. Bogomolov, S. V. Gaponenko, I. N. Gemnanenko, A. M. Kapitonov, E. P. Petrov, N. V. Gaponenko, A. V. Prokofiev, A. N. Ponyavina, N. I. Silvanovich, and S. M. Samoilovitch, Phys. Rev. E **55**, 7619 (1997).
[28] H. Miguez, C. Lopez, F. Meseguer, A. Blanco, L. Vazquez, R. Mayoral, M. Ocana, V. Fornes, and A. Mifsud, Appl. Phys. Lett. **71**, 1148 (1997).
[29] Judith E. G. J. Wijnhoven and Willem L. Vos, Science **281**, 802 (1998).
[30] A. A. Zakhidov *et al.*, Science **282**, 897 (1998).
[31] Yu. A. Vlasov, Nan Yao, and D. J. Norris, Adv. Mater. **11**, 165 (1999).
[32] B. R. Mollow, Phys. Rev. **188**, 1969 (1969).
[33] M. Lewenstein and T. W. Mossberg, Phys. Rev. A **38**, 808 (1988); J. Grochmalicki and M. Lewenstein, *ibid.* **40**, 2517 (1989).
[34] M. O. Scully, S. Y. Zhu, and A. Gavrielides, Phys. Rev. Lett. **62**, 2813 (1989); A. Imamoglu, Phys. Rev. A **40**, 2835 (1989).
[35] L. M. Narducci, M. O. Scully, G. L. Oppo, P. Ru, and J. R. Tredicce, Phys. Rev. A **42**, 1630 (1990); G. S. Agarwal, *ibid.* **54**, R3734 (1996).
[36] G. S. Agarwal, Phys. Rev. Lett. **67**, 980 (1991); S. Y. Zhu and M. O. Scully, *ibid.* **76**, 388 (1996).
[37] M. O. Scully, Phys. Rev. Lett. **67**, 1855 (1991); M. O. Scully and S. Y. Zhu, Opt. Commun. **87**, 134 (1992).
[38] S. E. Harris, J. E. Field, and A. Imamoglu, Phys. Rev. Lett. **64**, 1107 (1990).
[39] L. M. Narducci, H. M. Doss, P. Ru, M. O. Scully, S. Y. Zhu, and C. H. Keitel, Opt. Commun. **81**, 379 (1991).
[40] P. Brumer and M. Shapiro, Acc. Chem. Res. **22**, 407 (1989); C. Chen, Y-Y. Yin, and D. S. Elliot, Phys. Rev. Lett. **64**, 507 (1990); A. Shintman *et al.*, *ibid.* **76**, 2886 (1996).
[41] For a more detailed review, see *Coherence Phenomena in Atoms and Molecules in Laser Field*, edited by A. D. Bandrauk and S. C. Wallace (Plenum Press, New York, 1992).
[42] F. Wang, C. Chen, and D. S. Elliot, Phys. Rev. Lett. **77**, 2416 (1996).
[43] R. Atanasov, A. Haché, J. L. P. Hughes, H. M. van Driel, and J. E. Sipe, Phys. Rev. Lett. **76**, 1703 (1996).
[44] G. K. Brennen, C. M. Caves, P. S. Jessen, and I. H. Deutsch, Phys. Rev. Lett. **82**, 1060 (1999).
[45] S. Bay, P. Lambropoulos, and K. Molmer, Opt. Commun. **132**, 237 (1996).
[46] C. C. Gerry and J. H. Eberly, Phys. Rev. A **42**, 6805 (1990).
[47] O. Toader (private communication).
[48] P. Meystre and M. Sargent III, *Elements of Quantum Optics* (Spring-Verlag, New York, 1991); M. O. Scully and S. Zubairy, *Quantum Optics* (Cambridge University Press, London, 1997).
[49] N. Vats and S. John, Phys. Rev. A **58**, 4168 (1998).
[50] G. A. Korn and T. M. Korn, *Mathematical Handbook for Scientists and Engineers* (McGraw-Hill, New York, 1968), p. 17.
[51] J. J. Sanchez-Mondragon, N. B. Narozhny, and J. H. Eberly, Phys. Rev. Lett. **51**, 550 (1983).
[52] S. H. Autler and C. H. Townes, Phys. Rev. **100**, 703 (1955).
[53] T. Quang, M. Woldeyohannes, S. John, and G. S. Agarwal, Phys. Rev. Lett. **79**, 5238 (1997).
[54] D. DiVincenzo and B. Terhal, Phys. World **11**, 53 (1998).
[55] Shi-Yao Zhu, Ricky C. F. Chan, and Chin Pang Lee, Phys. Rev. A **52**, 710 (1995).
[56] Shi-Yao Zhu, Hong Chen, and Hu Huang, Phys. Rev. Lett. **79**, 205 (1997).
[57] P. J. Davis and P. Rabinowitz, *Methods of Numerical Integration*, 2nd ed. (Academic Press, New York, 1984).
[58] S. John and Tran Quang, Phys. Rev. Lett. **76**, 1320 (1996).
[59] N. Vats, K. Busch, and S. John (unpublished).
[60] S. Lanzerstorter *et al.*, Appl. Phys. Lett. **72**, 809 (1998); V. F. Masterov *et al.*, *ibid.* **72**, 728 (1998); Xinwei Zhao *et al.*, *ibid.* **74**, 120 (1999); S. Komuro *et al.*, *ibid.* **74**, 377 (1999).
[61] Claude N. Cohen-Tannoudji and William D. Phillips, Phys. Today **43**, 33 (1990).
[62] D. Gammon, E. S. Snow, and D. S. Katzer, Appl. Phys. Lett. **67**, 2391 (1995).
[63] N. H. Bonadeo, J. Erland, D. Gammon, D. Park, D. S. Katzer, and D. G. Steel, Science **282**, 1473 (1998), and references therein.
[64] U. Bockelmann and G. Bastard, Phys. Rev. B **42**, 8947 (1990).
[65] D. S. Citrin, Phys. Rev. B **47**, 3832 (1993).
[66] H. A. Bethe, Phys. Rev. **72**, 339 (1947).
[67] I. S. Gradshteyn and I. M. Ryzhik, *Table of Integrals, Series, and Products* (Academic, New York, 1980).